Chapter 7

SPIN WAVES IN NON-COLLINEAR SYSTEMS

7.1. Local Axis Transformation and Boson Hamiltonian

Until now, we have studied ferromagnetic systems where the spins are parallel in the ground state. As we have remarked in Chapter 1, other kinds of magnetic order have been observed in actual compounds as antiferromagnets, spiral and helix magnets. In this chapter, we will study Hamiltonian models that can give non-collinear configurations in the ground state. A non-collinear ground state can be obtained simply from the Heisenberg Hamiltonian (1.2.5) if the exchange interaction is not limited to NN spins.[54] Let us consider the exchange Hamiltonian

$$\mathcal{H} = -\sum_{i,\boldsymbol{\delta}_\alpha} J_\alpha \boldsymbol{S}_i \cdot \boldsymbol{S}_{i+\boldsymbol{\delta}_\alpha}, \tag{7.1.1}$$

where i runs over all sites of a Bravais lattice; J_α is the exchange integral between a spin located on the lattice site i and the shell of NN ($\alpha = 1$), NNN ($\alpha = 2$), third nearest neighbours (TNN) ($\alpha = 3$) and so on. In Eq. (7.1.1), $\boldsymbol{\delta}_\alpha$ is the set of vectors connecting the site i with its NN, NNN, TNN,... for $\alpha = 1, 2, 3, \ldots$, respectively. Let's assume that x, y, z are the crystal axes and introduce a reference system of local axes ξ, η, ζ, one for each lattice site. Suppose that each local axis ζ associated with the lattice site i lies on the surface of a cone characterized by an apex angle θ (independent of i), where θ is the angle between the crystal axis z and the local axis ζ. Then, suppose that the angle between the projections into the crystal xy-plane of the local axis ζ at the lattice sites i and j is $\boldsymbol{Q} \cdot (\boldsymbol{r}_i - \boldsymbol{r}_j)$ where $\boldsymbol{Q}$ is the helix wavevector. The more general relation between the components of the spin $\boldsymbol{S}_i$ along the crystal and local axes is given by

$$\begin{pmatrix} S_i^x \\ S_i^y \\ S_i^z \end{pmatrix} = \begin{pmatrix} \cos\theta\cos\phi_i & -\sin\phi_i & \sin\theta\cos\phi_i \\ \cos\theta\sin\phi_i & \cos\phi_i & \sin\theta\sin\phi_i \\ -\sin\theta & 0 & \cos\theta \end{pmatrix} \begin{pmatrix} S_i^\xi \\ S_i^\eta \\ S_i^\zeta \end{pmatrix}, \tag{7.1.2}$$

where $\phi_i = \boldsymbol{Q} \cdot \boldsymbol{r}_i + \phi$. Note that if the spin was a classic vector of magnitude S directed along the ζ-axis, Eq. (7.1.2) should become

$$\begin{aligned} S_i^x &= S \sin\theta \cos(\boldsymbol{Q} \cdot \boldsymbol{r}_i + \phi), \\ S_i^y &= S \sin\theta \sin(\boldsymbol{Q} \cdot \boldsymbol{r}_i + \phi), \\ S_i^z &= S \cos\theta \end{aligned} \tag{7.1.3}$$

corresponding to the usual representation of a vector $\boldsymbol{S}$ in spherical coordinates. Using the transformation (7.1.2) and writing the operators S_i^ξ and S_i^η in terms of the raising and lowering operators S_i^+ and S_i^- given by Eq. (1.3.3), the Hamiltonian (7.1.1) becomes

$$\begin{aligned} \mathcal{H} = -\sum_{i,\boldsymbol{\delta}_\alpha} J_\alpha \Big\{ & \left(\sin^2\theta \cos \boldsymbol{Q} \cdot \boldsymbol{\delta}_\alpha + \cos^2\theta\right) S_i^\zeta S_{i+\boldsymbol{\delta}_\alpha}^\zeta \\ & + \frac{1}{4}\sin^2\theta (1 - \cos \boldsymbol{Q} \cdot \boldsymbol{\delta}_\alpha)(S_i^+ S_{i+\boldsymbol{\delta}_\alpha}^+ + S_i^- S_{i+\boldsymbol{\delta}_\alpha}^-) \\ & + \frac{1}{4}[(1 + \cos^2\theta)\cos \boldsymbol{Q} \cdot \boldsymbol{\delta}_\alpha + \sin^2\theta - 2\, i \cos\theta \sin \boldsymbol{Q} \cdot \boldsymbol{\delta}_\alpha] S_i^+ S_{i+\boldsymbol{\delta}_\alpha}^- \\ & + \frac{1}{4}[(1 + \cos^2\theta)\cos \boldsymbol{Q} \cdot \boldsymbol{\delta}_\alpha + \sin^2\theta + 2\, i \cos\theta \sin \boldsymbol{Q} \cdot \boldsymbol{\delta}_\alpha] S_i^- S_{i+\boldsymbol{\delta}_\alpha}^+ \\ & - \frac{1}{2}\sin\theta [\cos\theta (1 - \cos \boldsymbol{Q} \cdot \boldsymbol{\delta}_\alpha) - i \sin \boldsymbol{Q} \cdot \boldsymbol{\delta}_\alpha](S_i^\zeta S_{i+\boldsymbol{\delta}_\alpha}^+ + S_i^- S_{i+\boldsymbol{\delta}_\alpha}^\zeta) \\ & - \frac{1}{2}\sin\theta [\cos\theta (1 - \cos \boldsymbol{Q} \cdot \boldsymbol{\delta}_\alpha) + i \sin \boldsymbol{Q} \cdot \boldsymbol{\delta}_\alpha](S_i^\zeta S_{i+\boldsymbol{\delta}_\alpha}^- + S_i^+ S_{i+\boldsymbol{\delta}_\alpha}^\zeta) \Big\}, \end{aligned} \tag{7.1.4}$$

where the parameters θ and $\boldsymbol{Q}$ have to be determined by a minimization of the ground-state energy. Note that the angle ϕ does not appear in the Hamiltonian (7.1.4). The presence of the angle θ in Eq. (7.1.4) is a consequence of the broken symmetry entered by the choice of the z-axis as the cone axis, while the absence of the angle ϕ reflects the invariance of the Hamiltonian under rotation about the z-axis. Obviously, the choice of the z-axis as the cone axis is arbitrary for the isotropic Heisenberg Hamiltonian (7.1.1). Only the anisotropic terms entered by the crystal field may fix the cone axis and the phase angle ϕ. By means of the transformation to the local axes given by Eq. (7.1.2), we can investigate the occurrence of non-collinear configurations. Replacing the local spin operators S_i^+, S_i^- and S_i^ζ by the boson creation and destruction operators using the spin-boson DM transformation given by (2.1.7), and using the Fourier transforms (2.2.14), one obtains

$$\mathcal{H} = E_0 + \sum_{n=1}^{6} \mathcal{H}_n, \tag{7.1.5}$$

where

$$E_0 = -\sum_{\boldsymbol{\delta}_\alpha} J_\alpha S^2 N (\sin^2\theta \cos \boldsymbol{Q} \cdot \boldsymbol{\delta}_\alpha + \cos^2\theta) \tag{7.1.6}$$

is the zeroth-order ground-state energy which is the "exact" ground-state energy only in the "classical limit" $S \to \infty$. Except for the isotropic ferromagnet the ground state of the Hamiltonian (7.1.1) is generally not known. An example was given in Chapter 6 where we have studied the planar ferromagnet. In the present case, a series of contributions ordered in powers of $\frac{1}{S}$ come from the interaction Hamiltonians $\mathcal{H}_n$ when a systematic perturbative theory is performed:

$$\mathcal{H}_1 = S\sqrt{2SN}\cos\theta\sin\theta\sum_{\boldsymbol{\delta}_\alpha} J_\alpha(1-\cos\boldsymbol{Q}\cdot\boldsymbol{\delta}_\alpha)(a_0+a_0^+) \tag{7.1.7}$$

is the linear term that will disappear when the minimum conditions of E_0 with respect to θ and $\boldsymbol{Q}$ will be taken into account:

$$\mathcal{H}_2 = \sum_{\boldsymbol{k}} A_{\boldsymbol{k}} a_{\boldsymbol{k}}^+ a_{\boldsymbol{k}} + \frac{1}{2}\sum_{\boldsymbol{k}} B_{\boldsymbol{k}}(a_{\boldsymbol{k}}a_{-\boldsymbol{k}} + a_{\boldsymbol{k}}^+ a_{-\boldsymbol{k}}^+) \tag{7.1.8}$$

with

$$A_{\boldsymbol{k}} = \sum_{\boldsymbol{\delta}_\alpha} 2J_\alpha S\Big\{ \sin^2\theta\cos\boldsymbol{Q}\cdot\boldsymbol{\delta}_\alpha + \cos^2\theta - \frac{1}{2}\cos\boldsymbol{k}\cdot\boldsymbol{\delta}_\alpha[\sin^2\theta + (1+\cos^2\theta)\cos\boldsymbol{Q}\cdot\boldsymbol{\delta}_\alpha] + \cos\theta\sin\boldsymbol{k}\cdot\boldsymbol{\delta}_\alpha\sin\boldsymbol{Q}\cdot\boldsymbol{\delta}_\alpha\Big\} \tag{7.1.9}$$

and

$$B_{\boldsymbol{k}} = -\sum_{\boldsymbol{\delta}_\alpha} J_\alpha S\sin^2\theta\cos\boldsymbol{k}\cdot\boldsymbol{\delta}_\alpha(1-\cos\boldsymbol{Q}\cdot\boldsymbol{\delta}_\alpha) \tag{7.1.10}$$

is the bilinear Hamiltonian that describes the system in the absence of interaction between the spin waves. From Eq. (7.1.9), one sees that $A_{\boldsymbol{k}} \neq A_{-\boldsymbol{k}}$. The remaining terms come from the interaction between the spin waves:

$$\mathcal{H}_3 = -\frac{1}{N}\sum_{\boldsymbol{k}_1,\boldsymbol{k}_2,\boldsymbol{k}_3}\left[\frac{1}{2}\sqrt{2SN}\cos\theta\sin\theta\sum_{\boldsymbol{\delta}_\alpha} J_\alpha\,(1-\cos\boldsymbol{Q}\cdot\boldsymbol{\delta}_\alpha) + C_{\boldsymbol{k}_3}\right] \times \delta_{\boldsymbol{k}_1,\boldsymbol{k}_2+\boldsymbol{k}_3}\; a_{\boldsymbol{k}_1}^+ a_{\boldsymbol{k}_2} a_{\boldsymbol{k}_3} - \frac{1}{N}\sum_{\boldsymbol{k}_1,\boldsymbol{k}_2,\boldsymbol{k}_3} C_{\boldsymbol{k}_1}\;\delta_{\boldsymbol{k}_1+\boldsymbol{k}_2,\boldsymbol{k}_3}\; a_{\boldsymbol{k}_1}^+ a_{\boldsymbol{k}_2}^+ a_{\boldsymbol{k}_3} \tag{7.1.11}$$

with

$$C_{\boldsymbol{k}} = \sqrt{2SN}\sin\theta\sum_{\boldsymbol{\delta}_\alpha} J_\alpha[\cos\theta\cos\boldsymbol{k}\cdot\boldsymbol{\delta}_\alpha(1-\cos\boldsymbol{Q}\cdot\boldsymbol{\delta}_\alpha) + \sin\boldsymbol{k}\cdot\boldsymbol{\delta}_\alpha\sin\boldsymbol{Q}\cdot\boldsymbol{\delta}_\alpha], \tag{7.1.12}$$

$$\mathcal{H}_4 = -\frac{1}{N}\sum_{\boldsymbol{k}_1,\boldsymbol{k}_2,\boldsymbol{k}_3,\boldsymbol{k}_4} V_{\boldsymbol{k}_1,\boldsymbol{k}_2,\boldsymbol{k}_3,\boldsymbol{k}_4}\;\delta_{\boldsymbol{k}_1+\boldsymbol{k}_2,\boldsymbol{k}_3+\boldsymbol{k}_4}\; a_{\boldsymbol{k}_1}^+ a_{\boldsymbol{k}_2}^+ a_{\boldsymbol{k}_3} a_{\boldsymbol{k}_4} - \frac{1}{2SN}\sum_{\boldsymbol{k}_1,\boldsymbol{k}_2,\boldsymbol{k}_3,\boldsymbol{k}_4} B_{\boldsymbol{k}_4}\;\delta_{\boldsymbol{k}_1,\boldsymbol{k}_2+\boldsymbol{k}_3+\boldsymbol{k}_4}\; a_{\boldsymbol{k}_1}^+ a_{\boldsymbol{k}_2} a_{\boldsymbol{k}_3} a_{\boldsymbol{k}_4} \tag{7.1.13}$$

with

$$V_{\boldsymbol{k}_1,\boldsymbol{k}_2,\boldsymbol{k}_3,\boldsymbol{k}_4} = \sum_{\boldsymbol{\delta}_\alpha} J_\alpha \Big\{ \cos[(\boldsymbol{k}_2 - \boldsymbol{k}_4)\cdot\boldsymbol{\delta}_\alpha](\sin^2\theta\cos\boldsymbol{Q}\cdot\boldsymbol{\delta}_\alpha + \cos^2\theta)$$
$$-\frac{1}{2}\cos\boldsymbol{k}_1\cdot\boldsymbol{\delta}_\alpha[(1+\cos^2\theta)\cos\boldsymbol{Q}\cdot\boldsymbol{\delta}_\alpha + \sin^2\theta]$$
$$+\cos\theta\sin\boldsymbol{k}_1\cdot\boldsymbol{\delta}_\alpha\sin\boldsymbol{Q}\cdot\boldsymbol{\delta}_\alpha\Big\}, \tag{7.1.14}$$

$$\mathcal{H}_5 = \frac{1}{2S^2N}\sum_{\boldsymbol{k}_1,\boldsymbol{k}_2,\boldsymbol{k}_3,\boldsymbol{k}_4,\boldsymbol{k}_5} C_{\boldsymbol{k}_1-\boldsymbol{k}_3}\ \delta_{\boldsymbol{k}_1+\boldsymbol{k}_2,\boldsymbol{k}_3+\boldsymbol{k}_4+\boldsymbol{k}_5}\ a^+_{\boldsymbol{k}_1}a^+_{\boldsymbol{k}_2}a_{\boldsymbol{k}_3}a_{\boldsymbol{k}_4}a_{\boldsymbol{k}_5} \tag{7.1.15}$$

and

$$\mathcal{H}_6 = \frac{1}{8S^2N^2}\sum_{\boldsymbol{k}_1,\boldsymbol{k}_2,\boldsymbol{k}_3,\boldsymbol{k}_4,\boldsymbol{k}_5,\boldsymbol{k}_6} B_{\boldsymbol{k}_1-\boldsymbol{k}_5-\boldsymbol{k}_6}\ \delta_{\boldsymbol{k}_1+\boldsymbol{k}_2,\boldsymbol{k}_3+\boldsymbol{k}_4+\boldsymbol{k}_5+\boldsymbol{k}_6}\ a^+_{\boldsymbol{k}_1}a^+_{\boldsymbol{k}_2}a_{\boldsymbol{k}_3}a_{\boldsymbol{k}_4}a_{\boldsymbol{k}_5}a_{\boldsymbol{k}_6}. \tag{7.1.16}$$

As noted in Chapters 2 and 6, the DM transformation generates only a finite number of interaction potentials even though the boson Hamiltonian so obtained is no longer hermitian. Let us perform the same steps on the anisotropic Hamiltonian

$$\mathcal{H}_{\rm an} = -h\sum_i S^z_i + D\sum_i (S^z_i)^2 \tag{7.1.17}$$

that accounts for an external uniform magnetic field directed along the z-axis $h = g\mu_B H$ and a single-ion easy-plane $D > 0$ anisotropy that forces the spins in the xy-plane. One obtains

$$\mathcal{H}_{\rm an} = E^{\rm an}_0 + \sum_{n=1}^{6}\mathcal{H}^{\rm an}_n, \tag{7.1.18}$$

where

$$E^{\rm an}_0 = DS^2N\left(1-\frac{1}{2S}\right)\cos^2\theta + \frac{1}{2}DSN - hSN\cos\theta, \tag{7.1.19}$$

$$\mathcal{H}^{\rm an}_1 = -\frac{1}{2}\sqrt{2SN}\sin\theta[D(2S-1)\cos\theta - h](a_0 + a^+_0), \tag{7.1.20}$$

$$\mathcal{H}^{\rm an}_2 = \left[DS\left(1-\frac{1}{2S}\right)(1-3\cos^2\theta) + h\cos\theta\right]\sum_{\boldsymbol{k}} a^+_{\boldsymbol{k}}a_{\boldsymbol{k}}$$
$$+\frac{1}{2}DS\left(1-\frac{1}{2S}\right)\sin^2\theta\sum_{\boldsymbol{k}}(a_{\boldsymbol{k}}a_{-\boldsymbol{k}} + a^+_{\boldsymbol{k}}a^+_{-\boldsymbol{k}}), \tag{7.1.21}$$

$$\mathcal{H}_2^{\rm NH} = \frac{D}{4}\sin^2\theta \sum_{\boldsymbol{k}} a_{\boldsymbol{k}}^+ a_{-\boldsymbol{k}}^+, \tag{7.1.22}$$

$$\begin{aligned}\mathcal{H}_3^{\rm an} = {} & D\sqrt{2SN}\cos\theta\sin\theta\frac{1}{N}\sum_{\boldsymbol{k}_1,\boldsymbol{k}_2,\boldsymbol{k}_3}\delta_{\boldsymbol{k}_1+\boldsymbol{k}_2,\boldsymbol{k}_3}a_{\boldsymbol{k}_1}^+ a_{\boldsymbol{k}_2}^+ a_{\boldsymbol{k}_3} \\ & + \sqrt{2SN}\sin\theta\frac{1}{N}\sum_{\boldsymbol{k}_1,\boldsymbol{k}_2,\boldsymbol{k}_3}\left[D\left(1-\frac{3}{4S}\right)\cos\theta - \frac{h}{4S}\right]\delta_{\boldsymbol{k}_1,\boldsymbol{k}_2+\boldsymbol{k}_3}\; a_{\boldsymbol{k}_1}^+ a_{\boldsymbol{k}_2} a_{\boldsymbol{k}_3},\end{aligned} \tag{7.1.23}$$

$$\begin{aligned}\mathcal{H}_4^{\rm an} = {} & -\frac{D}{2}\left(1-3\cos^2\theta\right)\frac{1}{N}\sum_{\boldsymbol{k}_1,\boldsymbol{k}_2,\boldsymbol{k}_3,\boldsymbol{k}_4}\delta_{\boldsymbol{k}_1+\boldsymbol{k}_2,\boldsymbol{k}_3+\boldsymbol{k}_4}\; a_{\boldsymbol{k}_1}^+ a_{\boldsymbol{k}_2}^+ a_{\boldsymbol{k}_3} a_{\boldsymbol{k}_4} \\ & - \sin^2\theta\frac{D}{2N}\left(1-\frac{1}{2S}\right)\sum_{\boldsymbol{k}_1,\boldsymbol{k}_2,\boldsymbol{k}_3,\boldsymbol{k}_4}\delta_{\boldsymbol{k}_1,\boldsymbol{k}_2+\boldsymbol{k}_3+\boldsymbol{k}_4}\; a_{\boldsymbol{k}_1}^+ a_{\boldsymbol{k}_2} a_{\boldsymbol{k}_3} a_{\boldsymbol{k}_4},\end{aligned} \tag{7.1.24}$$

$$\mathcal{H}_5^{\rm an} = -\sqrt{2SN}\cos\theta\sin\theta\frac{D}{4S^2N}\sum_{\boldsymbol{k}_1,\boldsymbol{k}_2,\boldsymbol{k}_3,\boldsymbol{k}_4,\boldsymbol{k}_5}\delta_{\boldsymbol{k}_1+\boldsymbol{k}_2,\boldsymbol{k}_3+\boldsymbol{k}_4+\boldsymbol{k}_5}\; a_{\boldsymbol{k}_1}^+ a_{\boldsymbol{k}_2}^+ a_{\boldsymbol{k}_3} a_{\boldsymbol{k}_4} a_{\boldsymbol{k}_5} \tag{7.1.25}$$

and

$$\mathcal{H}_6^{\rm an} = \sin^2\theta\frac{D}{8SN^2}\sum_{\boldsymbol{k}_1,\boldsymbol{k}_2,\boldsymbol{k}_3,\boldsymbol{k}_4,\boldsymbol{k}_5,\boldsymbol{k}_6}\delta_{\boldsymbol{k}_1+\boldsymbol{k}_2,\boldsymbol{k}_3+\boldsymbol{k}_4+\boldsymbol{k}_5+\boldsymbol{k}_6}\; a_{\boldsymbol{k}_1}^+ a_{\boldsymbol{k}_2}^+ a_{\boldsymbol{k}_3} a_{\boldsymbol{k}_4} a_{\boldsymbol{k}_5} a_{\boldsymbol{k}_6}. \tag{7.1.26}$$

Note that the anisotropic Hamiltonian (7.1.18) is independent of $\boldsymbol{Q}$ and ϕ. Consequently, the helix wavevector $\boldsymbol{Q}$ is determined only by the exchange Hamiltonian (7.1.5). Moreover, the ϕ angle cannot be selected by the anisotropic Hamiltonian (7.1.18) which is invariant under rotation about the z-axis. As we have seen in Chapter 6, the DM spin-boson transformation leads to a non-hermitian bilinear Hamiltonian (7.1.22). As for the isotropic contribution, however, the non-hermiticity appears only in the interaction potentials between spin waves. In Chapter 6, we have seen that a careful treatment of the terms of the same order in $\frac{1}{S}$ prevents any unphysical effect due to the non-hermiticity of the bilinear Hamiltonian. According to Chapter 6, we choose the unperturbed Hamiltonian as the hermitian contribution of the Hamiltonian bilinear $\mathcal{H}_2+\mathcal{H}_2^{\rm an}$ with $\mathcal{H}_2$ and $\mathcal{H}_2^{\rm an}$ given by Eqs. (7.1.8) and (7.1.21), respectively. A novelty with respect to the Hamiltonian of the planar ferromagnet is the presence of linear terms $\mathcal{H}_1+\mathcal{H}_1^{\rm an}$ containing a single Bose operator and of cubic terms $\mathcal{H}_3+\mathcal{H}_3^{\rm an}$ containing three Bose operators. While the linear term disappears when the minimum conditions are taken into account, the cubic terms do not vanish. Moreover, the cubic terms treated at the second-order in the $\frac{1}{S}$ perturbation expansion give a contribution of the same order of the quartic term $\mathcal{H}_4+\mathcal{H}_4^{\rm an}$ treated at the first-order. Like for the planar ferromagnet, a careful treatment of the perturbative terms has to be done.

7.2. Harmonic Approximation and Bogoliubov Transformation

Let us begin diagonalizing the isotropic bilinear Hamiltonian (7.1.8). From Eq. (7.1.9), we see that $A_{\boldsymbol{k}} \neq A_{-\boldsymbol{k}}$ so that it is convenient to write the Hamiltonian (7.1.8) in the more symmetric form

$$\mathcal{H}_2 = \frac{1}{2}\sum_{\boldsymbol{k}}[A_{\boldsymbol{k}}a^+_{\boldsymbol{k}}a_{\boldsymbol{k}} + A_{-\boldsymbol{k}}a^+_{-\boldsymbol{k}}a_{-\boldsymbol{k}} + B_{\boldsymbol{k}}(a_{\boldsymbol{k}}a_{-\boldsymbol{k}} + a^+_{\boldsymbol{k}}a^+_{-\boldsymbol{k}})] \tag{7.2.1}$$

before introducing the Bogoliubov transformation (6.1.14)

$$a_{\boldsymbol{k}} = l_{\boldsymbol{k}}(\alpha_{\boldsymbol{k}} - x_{\boldsymbol{k}}\alpha^+_{-\boldsymbol{k}}), \quad a^+_{\boldsymbol{k}} = l_{\boldsymbol{k}}(\alpha^+_{\boldsymbol{k}} - x_{\boldsymbol{k}}\alpha_{-\boldsymbol{k}}) \tag{7.2.2}$$

where

$$l^2_{\boldsymbol{k}}(1 - x^2_{\boldsymbol{k}}) = 1. \tag{7.2.3}$$

By means of the Bogoliubov transformation (7.2.2), the Hamiltonian (7.2.1) becomes

$$\begin{aligned}\mathcal{H}_2 = \sum_{\boldsymbol{k}} l^2_{\boldsymbol{k}}\{&[A^{(\mathrm{s})}_{\boldsymbol{k}} + A^{(\mathrm{a})}_{\boldsymbol{k}} + (A^{(\mathrm{s})}_{\boldsymbol{k}} - A^{(\mathrm{a})}_{\boldsymbol{k}})x^2_{\boldsymbol{k}} - 2B_{\boldsymbol{k}}x_{\boldsymbol{k}}]\alpha^+_{\boldsymbol{k}}\alpha_{\boldsymbol{k}} \\ &+ [-2A^{(\mathrm{s})}_{\boldsymbol{k}}x_{\boldsymbol{k}} + B_{\boldsymbol{k}}(1 + x^2_{\boldsymbol{k}})]\frac{1}{2}(\alpha_{\boldsymbol{k}}\alpha_{-\boldsymbol{k}} + \alpha^+_{\boldsymbol{k}}\alpha^+_{-\boldsymbol{k}}) + A^{(\mathrm{s})}_{\boldsymbol{k}}x^2_{\boldsymbol{k}} - B_{\boldsymbol{k}}x_{\boldsymbol{k}}\}\end{aligned} \tag{7.2.4}$$

where

$$\begin{aligned}A^{(\mathrm{s})}_{\boldsymbol{k}} = \frac{1}{2}(A_{\boldsymbol{k}} + A_{-\boldsymbol{k}}) = \sum_{\boldsymbol{\delta}_\alpha} 2J_\alpha S \Big\{ &\sin^2\theta\cos\boldsymbol{Q}\cdot\boldsymbol{\delta}_\alpha + \cos^2\theta \\ &-\frac{1}{2}\cos\boldsymbol{k}\cdot\boldsymbol{\delta}_\alpha[\sin^2\theta + (1+\cos^2\theta)\cos\boldsymbol{Q}\cdot\boldsymbol{\delta}_\alpha]\Big\}\end{aligned} \tag{7.2.5}$$

and

$$A^{(\mathrm{a})}_{\boldsymbol{k}} = \frac{1}{2}(A_{\boldsymbol{k}} - A_{-\boldsymbol{k}}) = \cos\theta\sum_{\boldsymbol{\delta}_\alpha} 2J_\alpha S\sin\boldsymbol{k}\cdot\boldsymbol{\delta}_\alpha\sin\boldsymbol{Q}\cdot\boldsymbol{\delta}_\alpha. \tag{7.2.6}$$

The Hamiltonian (7.2.4) is diagonalized if $x_{\boldsymbol{k}}$ satisfies the equation

$$-2A^{(\mathrm{s})}_{\boldsymbol{k}}x_{\boldsymbol{k}} + B_{\boldsymbol{k}}(1 + x^2_{\boldsymbol{k}}) = 0. \tag{7.2.7}$$

The solutions of Eq. (7.2.7) are

$$x_{\boldsymbol{k}} = \frac{A^{(\mathrm{s})}_{\boldsymbol{k}} \pm \sqrt{A^{(\mathrm{s})2}_{\boldsymbol{k}} - B^2_{\boldsymbol{k}}}}{B_{\boldsymbol{k}}}. \tag{7.2.8}$$

Replacing the solutions given by Eqs. (7.2.8) in Eq. (7.2.3), one can see that the solution with the + sign leads to a $l^2_{\boldsymbol{k}} < 0$ so that it has to be rejected. On the

contrary, the solution with the − sign leads to

$$l_{\boldsymbol{k}}^2 = \frac{1}{2}\left(\frac{A_{\boldsymbol{k}}^{(\mathrm{s})}}{\sqrt{A_{\boldsymbol{k}}^{(\mathrm{s})2} - B_{\boldsymbol{k}}^2}} + 1\right), \tag{7.2.9}$$

$$l_{\boldsymbol{k}}^2 x_{\boldsymbol{k}} = \frac{1}{2}\frac{B_{\boldsymbol{k}}}{\sqrt{A_{\boldsymbol{k}}^{(\mathrm{s})2} - B_{\boldsymbol{k}}^2}}, \tag{7.2.10}$$

$$l_{\boldsymbol{k}}^2 x_{\boldsymbol{k}}^2 = \frac{1}{2}\left(\frac{A_{\boldsymbol{k}}^{(\mathrm{s})}}{\sqrt{A_{\boldsymbol{k}}^{(\mathrm{s})2} - B_{\boldsymbol{k}}^2}} - 1\right) \tag{7.2.11}$$

and the Hamiltonian (7.2.4) becomes

$$\mathcal{H}_2 = \sum_{\boldsymbol{k}}\left(\sqrt{A_{\boldsymbol{k}}^{(\mathrm{s})2} - B_{\boldsymbol{k}}^2} + A_{\boldsymbol{k}}^{(\mathrm{a})}\right)\alpha_{\boldsymbol{k}}^{+}\alpha_{\boldsymbol{k}} + \frac{1}{2}\sum_{\boldsymbol{k}}\left(\sqrt{A_{\boldsymbol{k}}^{(\mathrm{s})2} - B_{\boldsymbol{k}}^2} - A_{\boldsymbol{k}}^{(\mathrm{s})}\right). \tag{7.2.12}$$

By means of the definitions

$$S_{\boldsymbol{k}} = A_{\boldsymbol{k}}^{(\mathrm{s})} + B_{\boldsymbol{k}} = \sum_{\boldsymbol{\delta}_\alpha} 2J_\alpha S[\sin^2\theta(\cos\boldsymbol{Q}\cdot\boldsymbol{\delta}_\alpha - \cos\boldsymbol{k}\cdot\boldsymbol{\delta}_\alpha) + \cos^2\theta(1 - \cos\boldsymbol{k}\cdot\boldsymbol{\delta}_\alpha\cos\boldsymbol{Q}\cdot\boldsymbol{\delta}_\alpha)] \tag{7.2.13}$$

and

$$D_{\boldsymbol{k}} = A_{\boldsymbol{k}}^{(\mathrm{s})} - B_{\boldsymbol{k}} = \sum_{\boldsymbol{\delta}_\alpha} 2J_\alpha S[\cos\boldsymbol{Q}\cdot\boldsymbol{\delta}_\alpha(1 - \cos\boldsymbol{k}\cdot\boldsymbol{\delta}_\alpha) + \cos^2\theta(1 - \cos\mathbf{Q}\cdot\boldsymbol{\delta}_\alpha)] \tag{7.2.14}$$

the Hamiltonian (7.2.12) becomes

$$\mathcal{H}_2 = \Delta E_0 + \sum_{\boldsymbol{k}}\left(\sqrt{S_{\boldsymbol{k}}D_{\boldsymbol{k}}} + A_{\boldsymbol{k}}^{(\mathrm{a})}\right)\alpha_{\boldsymbol{k}}^{+}\alpha_{\boldsymbol{k}} \tag{7.2.15}$$

where

$$\Delta E_0 = \frac{1}{2}\sum_{\boldsymbol{k}}\left(\sqrt{S_{\boldsymbol{k}}D_{\boldsymbol{k}}} - A_{\boldsymbol{k}}^{(\mathrm{s})}\right) \tag{7.2.16}$$

is the first quantum correction of order $\frac{1}{S}$ with respect to the classical ground-state energy E_0 given by Eq. (7.1.6).

Taking the anisotropic bilinear Hamiltonian (7.1.21) into account, Eqs. (7.2.13) and (7.2.14) do not change if $S_{\boldsymbol{k}}$ and $D_{\boldsymbol{k}}$ are replaced by

$$S_{\boldsymbol{k}}^{\mathrm{an}} = S_{\boldsymbol{k}} + 2DS\left(1 - \frac{1}{2S}\right)(1 - 2\cos^2\theta) + h\cos\theta \tag{7.2.17}$$

and

$$D_{\boldsymbol{k}}^{\mathrm{an}} = D_{\boldsymbol{k}} - 2DS\left(1 - \frac{1}{2S}\right)\cos^2\theta + h\cos\theta, \tag{7.2.18}$$

respectively.

7.3. Ground-State Configurations

The zero-order approximation assumes that the ground-state energy is the absolute minimum of $E_{\rm G} = E_0 + E_0^{\rm an}$ with E_0 and $E_0^{\rm an}$ given by Eqs. (7.1.6) and (7.1.19), respectively. The absolute minimum of $E_{\rm G}$ has to be looked for among the simultaneous solutions of the equations $\frac{\partial E_G}{\partial \theta} = 0$ and $\frac{\partial E_G}{\partial Q_i} = 0$ with $i = x, y, z$ that is

$$\sin\theta \left\{ \cos\theta \left[\sum_{\boldsymbol{\delta}_\alpha} 2J_\alpha S(1 - \cos \boldsymbol{Q}\cdot\boldsymbol{\delta}_\alpha) - D(2S-1) \right] + h \right\} = 0 \tag{7.3.1}$$

and

$$\sin^2\theta \sum_{\boldsymbol{\delta}_\alpha} J_\alpha(\boldsymbol{\delta}_\alpha \cdot \mathbf{u}_i) \sin \boldsymbol{Q}\cdot\boldsymbol{\delta}_\alpha = 0, \quad i = x, y, z, \tag{7.3.2}$$

where $\mathbf{u}_i$ are the unit vectors along the $i = x, y, z$ axes. Note that Eq. (7.3.1) coincides with the vanishing of the linear term $\mathcal{H}_1 + \mathcal{H}_1^{\rm an}$ where $\mathcal{H}_1$ and $\mathcal{H}_1^{\rm an}$ are given by Eqs. (7.1.7) and (7.1.20), respectively. This general property confirms that linear terms in the boson Hamiltonian disappear when the ground state corresponds to an energy minimum. The minimum obtained from Eq. (7.3.1) is

$$\sin\theta = 0 \tag{7.3.3}$$

for $h > h_c$ and

$$\cos\theta = \frac{h}{h_c} \tag{7.3.4}$$

for $h \leq h_c$ where

$$h_c = D(2S-1) - \sum_{\boldsymbol{\delta}_\alpha} 2J_\alpha S(1 - \cos \boldsymbol{Q}\cdot\boldsymbol{\delta}_\alpha). \tag{7.3.5}$$

The solution (7.3.3) corresponds to the "saturated ferromagnetic" phase with all spins directed along the z-axis that is stable only in presence of magnetic fields strong enough. The solution (7.3.4) corresponds to a "cone structure" with an apex angle depending on the magnetic field that reduces to the saturated ferromagnetic phase for $h = h_c$ and to a regular "helix structure" with all spins lying in the xy-plane for $h = 0$. For $0 \leq h \leq h_c$, the spin wave spectrum is given by

$$\hbar\omega_{\boldsymbol{k}} = \sqrt{S_{\boldsymbol{k}}^{\rm an} D_{\boldsymbol{k}}^{\rm an}} + A_{\boldsymbol{k}}^{(\rm a)} \tag{7.3.6}$$

with

$$S_{\boldsymbol{k}}^{\rm an} = \sum_{\boldsymbol{\delta}_\alpha} 2J_\alpha S \left[\cos \boldsymbol{Q}\cdot\boldsymbol{\delta}_\alpha - \cos \boldsymbol{k}\cdot\boldsymbol{\delta}_\alpha + \left(\frac{h}{h_c}\right)^2 \cos \boldsymbol{k}\cdot\boldsymbol{\delta}_\alpha \,(1 - \cos \boldsymbol{Q}\cdot\boldsymbol{\delta}_\alpha) \right]$$

$$+ D(2S-1) \left[1 - \left(\frac{h}{h_c}\right)^2 \right], \tag{7.3.7}$$

$$D_{\boldsymbol{k}}^{\rm an} = \sum_{\boldsymbol{\delta}_\alpha} 2J_\alpha S \cos \boldsymbol{Q}\cdot\boldsymbol{\delta}_\alpha (1 - \cos \boldsymbol{k}\cdot\boldsymbol{\delta}_\alpha) \tag{7.3.8}$$

and

$$A_{\boldsymbol{k}}^{(\mathrm{a})} = \frac{h}{h_c} \sum_{\boldsymbol{\delta}_\alpha} 2J_\alpha S \sin \boldsymbol{k} \cdot \boldsymbol{\delta}_\alpha \sin \boldsymbol{Q} \cdot \boldsymbol{\delta}_\alpha. \tag{7.3.9}$$

Note that the spectrum (7.3.6) shows a soft mode at $\boldsymbol{k} = 0$ even in presence of an external magnetic field since Eq. (7.3.8) vanishes in that limit. The existence of the soft mode at $\boldsymbol{k} = 0$ is not restricted to the "unperturbed" spectrum (7.3.6) obtained from the bilinear Hamiltonian describing a collection of non-interacting spin waves. The soft mode remains also when the interactions between the spin waves are taken into account since it reflects the invariance of the total Hamiltonian under rotation about the magnetic field direction. Indeed, the existence of this soft mode was proved, in general, making use of a generalization of the Goldstone theorem.[55] For $h = 0$, the apex angle of the cone is $\frac{\pi}{2}$ and the ground-state configuration is a regular helix in which all spins rotate in the xy-plane with a pitch determined by the solutions of Eq. (7.3.2). The presence of a single-ion easy-plane anisotropy prevents the existence of a soft mode at $\boldsymbol{k} = \boldsymbol{Q}$ even for $h = 0$ since Eq. (7.3.7) vanishes only in the isotropic limit ($D = h = 0$). In this case, the existence of a soft mode at $\boldsymbol{k} = \boldsymbol{Q}$ reflects a more general property of the system[55] corresponding to the invariance of the isotropic Hamiltonian under a rotation of the plane where the spins lie. The spiral configurations ($0 < \theta < \frac{\pi}{2}$) observed in some rare earths[9,56] in the absence of an external magnetic field can be explained only by adding crystal field terms of higher order to the Heisenberg Hamiltonian. For Hamiltonians with single-ion easy-plane anisotropy, the regular helix phases are the only possible configurations. This theoretical expectation is confirmed by the experimental data on some transition metal halides like[57] $NiBr_2$ or[58] NiI_2 and CoI_2.

In order to find the helix wavevector, equations in (7.3.2) have to be investigated: They correspond to D equations to be solved simultaneously where D is the lattice dimensionality and they depend on the exchange interactions only.

From now on, we restrict to the isotropic case with the minimum of E_0 corresponding to $\theta = \frac{\pi}{2}$. The spin wave spectrum (7.3.6) reduces to

$$\hbar\omega_{\boldsymbol{k}} = \sqrt{S_{\boldsymbol{k}} D_{\boldsymbol{k}}} \tag{7.3.10}$$

since $A_{\boldsymbol{k}}^{(\mathrm{a})}$ given by Eq. (7.2.6) vanishes for $\theta = \frac{\pi}{2}$. Equations (7.2.12) and (7.2.13) become

$$S_{\boldsymbol{k}} = \sum_{\boldsymbol{\delta}_\alpha} 2J_\alpha S(\cos \boldsymbol{Q} \cdot \boldsymbol{\delta}_\alpha - \cos \boldsymbol{k} \cdot \boldsymbol{\delta}_\alpha) \tag{7.3.11}$$

and

$$D_{\boldsymbol{k}} = \sum_{\boldsymbol{\delta}_\alpha} 2J_\alpha S \cos \boldsymbol{Q} \cdot \boldsymbol{\delta}_\alpha (1 - \cos \boldsymbol{k} \cdot \boldsymbol{\delta}_\alpha). \tag{7.3.12}$$

From Eqs. (7.3.10)–(7.3.12), it is direct to see that there are two *soft modes* at $\boldsymbol{k} = 0$ and $\boldsymbol{k} = \boldsymbol{Q}$. Classically, the two soft modes correspond to a "uniform" rotation of

the spins in the xy-plane ($\boldsymbol{k} = 0$) and to a rigid rotation of the xy-plane around any straight line lying in the plane ($\boldsymbol{k} = \boldsymbol{Q}$).

Let us conclude this section evaluating the average value of the spin

$$\begin{aligned} \langle S_i^x \rangle &= \langle S_i^\zeta \rangle \cos(\boldsymbol{Q} \cdot \boldsymbol{r}_i + \phi), \\ \langle S_i^y \rangle &= \langle S_i^\zeta \rangle \sin(\boldsymbol{Q} \cdot \boldsymbol{r}_i + \phi), \\ \langle S_i^z \rangle &= 0, \end{aligned} \tag{7.3.13}$$

where

$$\begin{aligned} \langle S_i^\zeta \rangle &= S - \langle a_i^+ a_i \rangle = S \left(1 - \frac{1}{NS} \sum_{\boldsymbol{k}} \langle a_{\boldsymbol{k}}^+ a_{\boldsymbol{k}} \rangle \right) \\ &= S \left(1 - \frac{1}{2NS} \sum_{\boldsymbol{k}} \frac{A_{\boldsymbol{k}} - \hbar\omega_{\boldsymbol{k}}}{\hbar\omega_{\boldsymbol{k}}} - \frac{1}{NS} \sum_{\boldsymbol{k}} \frac{A_{\boldsymbol{k}}}{\hbar\omega_{\boldsymbol{k}}} \langle \alpha_{\boldsymbol{k}}^+ \alpha_{\boldsymbol{k}} \rangle \right), \end{aligned} \tag{7.3.14}$$

where $\hbar\omega_{\boldsymbol{k}}$ is given by Eq. (7.3.10) and $A_{\boldsymbol{k}}$ is given by Eq. (7.1.9) with $\theta = \frac{\pi}{2}$. As one can see, the average value of the spin is reduced with respect to its saturation value S even at zero temperature due to the existence of quantum fluctuations. The non saturation at zero temperature is called *spin reduction.*.

7.4. Néel Antiferromagnet

The exact ground-state wave function and the exact ground-state energy of an antiferromagnet are not known except for the LC with $S = \frac{1}{2}$ for which the famous solutions of Bethe[10] in 1931 for the wave function and of Hulthén[11] in 1938 for the energy are available. In this section, we will obtain the approximate antiferromagnetic ground state and the antiferromagnetic spin waves as a special case of a helix configuration. This procedure is not conventional but it is very simple. Let us consider the Hamiltonian (7.1.1) with a NN exchange interaction that is $J_\alpha = J < 0$ for $\alpha = 1$ and $J_\alpha = 0$ otherwise. Moreover, $\boldsymbol{\delta}_\alpha = \boldsymbol{\delta}$ for $\alpha = 1$ and zero otherwise. The classical ground-state energy E_0 obtained from Eqs. (7.1.6) with $\theta = \frac{\pi}{2}$ is

$$E_0 = |J| S^2 N \sum_{\boldsymbol{\delta}} \cos \boldsymbol{Q} \cdot \boldsymbol{\delta} = z|J| S^2 N \, \gamma_{\boldsymbol{Q}} \tag{7.4.1}$$

with $\gamma_{\boldsymbol{Q}}$ given by Eq. (2.2.17). We write explicitly the energy (7.4.1) for some loose packed lattices like the SQ lattice

$$E_0^{\mathrm{SQ}} = 2|J| S^2 N (\cos aQ_x + \cos aQ_y), \tag{7.4.2}$$

the SC lattice

$$E_0^{\mathrm{SC}} = 2|J| S^2 N (\cos aQ_x + \cos aQ_y + \cos aQ_z), \tag{7.4.3}$$

the BCC lattice

$$E_0^{\mathrm{BCC}} = 8|J| S^2 N \cos \frac{aQ_x}{2} \cos \frac{aQ_y}{2} \cos \frac{aQ_z}{2} \tag{7.4.4}$$

and the tetragonal (T) lattice

$$E_0^{\mathrm{T}} = 2|J|S^2N(\cos aQ_x + \cos aQ_y) + 2|J'|S^2N\cos cQ_z, \tag{7.4.5}$$

where J and J' are the NN antiferromagnetic exchange interactions in the xy-plane and out-of-plane, respectively. For these lattices, the helix wavevector corresponding to the absolute minimum of Eq. (7.4.1) is

$$\boldsymbol{Q}^{\mathrm{SQ}} = \left(\frac{\pi}{a}, \frac{\pi}{a}\right), \quad \boldsymbol{Q}^{\mathrm{SC}} = \left(\frac{\pi}{a}, \frac{\pi}{a}, \frac{\pi}{a}\right),$$

$$\boldsymbol{Q}^{\mathrm{BCC}} = \left(\frac{2\pi}{a}, \frac{2\pi}{a}, \frac{2\pi}{a}\right), \quad \boldsymbol{Q}^{\mathrm{T}} = \left(\frac{\pi}{a}, \frac{\pi}{a}, \frac{\pi}{c}\right) \tag{7.4.6}$$

so that, in general, the antiferromagnetic ground state for loose packed lattices corresponds to

$$\boldsymbol{Q} = \frac{1}{2}(\boldsymbol{a}^* + \boldsymbol{b}^* + \boldsymbol{c}^*), \quad \gamma_{\boldsymbol{Q}} = -1. \tag{7.4.7}$$

where $\boldsymbol{a}^*, \boldsymbol{b}^*, \boldsymbol{c}^*$ are the reciprocal lattice basic vectors. For instance, the reciprocal triad of the BCC lattice is

$$\boldsymbol{a}^* = \frac{2\pi}{a}(\mathbf{u}_x + \mathbf{u}_y), \quad \boldsymbol{b}^* = \frac{2\pi}{a}(\mathbf{u}_y + \mathbf{u}_z), \quad \boldsymbol{c}^* = \frac{2\pi}{a}(\mathbf{u}_z + \mathbf{u}_x). \tag{7.4.8}$$

The classical ground-state spin configuration can be easily obtained from Eq. (7.3.13) replacing $\langle S_i^\zeta \rangle$ with S. Since the generic lattice vector is given by

$$\boldsymbol{r}_{l,m,n} = l\boldsymbol{a} + m\boldsymbol{b} + n\boldsymbol{c}, \tag{7.4.9}$$

the generic spin vector located at the lattice site (l, m, n) becomes

$$\boldsymbol{S}_{l,m,n} = S\cos\left[(l+m+n)\pi + \phi\right]\mathbf{u}_x + S\sin\left[(l+m+n)\pi + \phi\right]\mathbf{u}_y \tag{7.4.10}$$

where Eq. (7.4.7) has been used. In Fig. 7.1, we show the classical ground-state configuration of the SQ lattice obtained from Eq. (7.4.10) with $n = 0$ and $\phi = \frac{\pi}{2}$. The kind of order shown in Fig. 7.1 is common to all *Néel antiferromagnets* in which the NN spins of a given spin are antiparallel to that spin. It should be noted that all the lattices considered in this section satisfy the condition $\mathbf{Q} \cdot \boldsymbol{\delta} = \pi$ that is peculiar of the Néel antiferromagnetic order. Making use of Eq. (7.4.7), the spin wave spectrum (7.3.10) becomes

$$\hbar\omega_{\boldsymbol{k}} = 2z|J|S\sqrt{1-\gamma_{\boldsymbol{k}}^2}, \tag{7.4.11}$$

where $\gamma_{\boldsymbol{k}}$ is given by Eq. (2.2.17). The spectrum (7.4.11) vanishes linearly with k in the long wavelength limit. In particular, for the cubic lattices one has

$$\hbar\omega_{\boldsymbol{k}} \sim 2|J|S\sqrt{2z}(ak) \tag{7.4.12}$$

and the free energy becomes

$$\begin{aligned} F &= E_{\mathrm{GS}} + k_BTN\frac{v_c}{8\pi^3}\int_{\mathrm{BZ}} d^3\boldsymbol{k}\ln(1 - e^{-\beta\hbar\omega_k}) \\ &= E_{\mathrm{GS}} + k_BTN\frac{m}{2\pi^2}\int_0^\infty k^2dk\ln(1 - e^{-\beta 2|J|S\sqrt{2z}k}), \end{aligned} \tag{7.4.13}$$

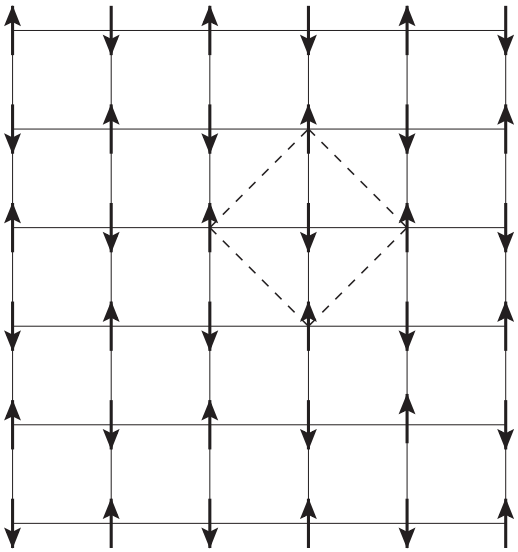

Fig. 7.1. Ground-state spin configuration for a SQ antiferromagnet. The dashed line represents the magnetic unit cell.

where $m = 2$ for the SC and $m = 1$ for the BCC lattice and

$$E_{\rm GS} = E_0 + \Delta E_0 = -z|J|S^2 N \left(1 + \frac{c}{S}\right) \tag{7.4.14}$$

where

$$c = \frac{1}{N} \sum_{\boldsymbol{k}} \left(1 - \sqrt{1 - \gamma_{\boldsymbol{k}}^2}\right) \tag{7.4.15}$$

is the first-order contribution to the zero-point energy. The numerical value[59] of c is 0.097 and 0.073 for the SC and BCC lattices, respectively. Equation (7.4.15) evaluated for a SQ lattice gives[59] $c = 0.158$ showing that the zero-point energy increases as the dimensionality decreases. This general trend is confirmed by evaluating Eq. (7.4.15) for the antiferromagnetic LC

$$c = \frac{1}{\pi} \int_0^{\pi} dk(1 - \sin k) = 1 - \frac{2}{\pi} = 0.363. \tag{7.4.16}$$

The exact ground-state energy[11] of the antiferromagnetic LC with $S = \frac{1}{2}$ is

$$E_{\rm GS} = \frac{1}{2}|J|N(1 - 4\ln 2) = -\frac{1}{2}|J|N\ 1.773 \tag{7.4.17}$$

while the first-order result (7.4.14) for $S = \frac{1}{2}$ and c given by Eq. (7.4.16) is

$$E_{\rm GS} = -\frac{1}{2}|J|N(1 + 2c) = -\frac{1}{2}|J|N\ 1.727 \tag{7.4.18}$$

pointing out that the first-order result is not so bad.

The temperature-dependent contribution of the free energy given by Eq. (7.4.13) can be evaluated using the series expansion of the logarithmic function

$$\ln(1-x) = -\sum_{n=1}^{\infty} \frac{x^n}{n} \tag{7.4.19}$$

by means of which Eq. (7.4.13) becomes

$$\begin{aligned} F &= E_{\rm GS} - k_B T N \frac{m}{2\pi^2} \sum_{n=1}^{\infty} \frac{1}{n} \int_0^{\infty} k^2 dk e^{-n\beta 2|J|S\sqrt{2z}\ k} \\ &= E_{\rm GS} - k_B T N \frac{m}{2\pi^2} (\beta 2|J|S\sqrt{2z})^{-3} \sum_{n=1}^{\infty} \frac{1}{n^4} \int_0^{\infty} dx x^2 e^{-x} \\ &= E_{\rm GS} - k_B T N \frac{\zeta(4)}{\pi^2} \eta \left(\frac{k_B T}{2z|J|S} \right)^3 \end{aligned} \tag{7.4.20}$$

where $\zeta(4) = \frac{\pi^4}{90}$; $\eta = 6\sqrt{3}$ and 8 for the SC and BCC lattices, respectively. The internal energy becomes

$$U = -T^2 \frac{\partial}{\partial T} \left(\frac{F}{T} \right) = E_{\rm GS} + 2z|J|SN \frac{3\zeta(4)}{\pi^2} \eta \left(\frac{k_B T}{2z|J|S} \right)^4. \tag{7.4.21}$$

The heat capacity becomes

$$C = \frac{\partial U}{\partial T} = k_B N \frac{12\zeta(4)}{\pi^2} \eta \left(\frac{k_B T}{2z|J|S} \right)^3. \tag{7.4.22}$$

As one can see from Eq. (7.4.22), the heat capacity of an antiferromagnet is proportional to T^3 at low temperature. This behaviour differs from that obtained for a ferromagnet $C \sim T^{3/2}$ given by Eq. (2.4.8). The reason is the different dispersion relation of the spin wave spectra in the long wavelength limit: linear for an antiferromagnet, quadratic for a ferromagnet. Experimentally, it is difficult to distinguish between the vibrational and magnetic contributions to the heat capacity of an antiferromagnet since both contributions are of the same order in temperature (T^3) in the low temperature limit. However, one can distinguish between the vibrational and magnetic contribution measuring the heat capacity of the sample *above* the Néel temperature T_N where the magnetic order disappears. Since, generally the Néel temperature is much lower than the Debye temperature, the cubic contribution to the heat capacity measured above T_N is entirely due to the lattice vibrations. Then, measuring the heat capacity of the sample below T_N and subtracting the vibrational contribution obtained from the "high" temperature experiment, one can distinguish between the magnetic and vibrational contribution.

The average value of the local spin at low temperature is

$$\langle S_i^\zeta \rangle = S\left(1 - \frac{c'}{2S} - \frac{1}{NS}\sum_{\boldsymbol{k}} \frac{n_{\boldsymbol{k}}}{\sqrt{1-\gamma_{\boldsymbol{k}}^2}}\right), \tag{7.4.23}$$

where

$$c' = \frac{1}{N}\sum_{\boldsymbol{k}}\left(\frac{1}{\sqrt{1-\gamma_{\boldsymbol{k}}^2}} - 1\right) \tag{7.4.24}$$

and

$$n_{\boldsymbol{k}} = \frac{1}{e^{\frac{2z|J|S}{k_B T}\sqrt{1-\gamma_{\boldsymbol{k}}^2}} - 1} \simeq \frac{1}{e^{\frac{2|J|S}{k_B T}\sqrt{2z}ak} - 1}. \tag{7.4.25}$$

The spin reduction c' that is the deviation from the saturation value S at zero temperature is given[59] by 0.156 and 0.119 for SC and BCC lattices, respectively. Like the zero-point energy also the spin reduction increases as the dimensionality decreases: for instance one finds[59] $c' = 0.394$ for a SQ lattice. For the LC, the sum in Eq. (7.4.24) diverges logarithmically pointing out that LRO is lost even at $T = 0$. Using the long wavelength approximation (7.4.25) in Eq. (7.4.23), the low temperature thermal average of the local spin becomes

$$\langle S_i^\zeta \rangle = S\left[1 - \frac{c'}{2S} - \frac{\zeta(2)}{2\pi^2 S}\eta\left(\frac{k_B T}{2z|J|S}\right)^2\right]. \tag{7.4.26}$$

The low temperature deviation from the zero temperature value of the local spin is proportional to T^2 to be compared with the deviation proportional to $T^{3/2}$ given by Eq. (2.4.11) for a ferromagnet. Also in this case the different low temperature behaviour of the ferromagnetic magnetization from the antiferromagnetic "sublattice" magnetization (the correct order parameter of the antiferromagnet since the total magnetization is always zero) is due to the different dispersion relation of the ferromagnetic and antiferromagnetic spin wave spectrum in the long wavelength limit..

For quasi-2D lattices characterized by a stacking of planes in which the exchange interaction between the spins in the plane $|J|$ is much larger than the exchange interaction between the NN spins belonging to different planes $|J'|$ the heat capacity is proportional to T^2 for $\sqrt{JJ'} < k_B T < |J|$ while the usual 3D behaviour $C \sim T^3$ is recovered for $k_B T < \sqrt{JJ'}$. Note that in many actual compounds this behaviour has been experimentally tested. In particular, for the BX_2 compounds,[60] where B is a 3*d*-transition metal like vanadium (V), manganese (Mn), iron (Fe), cobalt (Co) or nickel (Ni) and X is a halogen like bromine (Br), chlorine (Cl) or iodine (I) the in-plane exchange interaction is two order of magnitude greater than the out-of-plane exchange coupling. Moreover, in some of the "high-T_c superconductors" (HTCS)[61] like $La_{2-x}B_xCuO_{4-y}$ with B=Ca, Sr or Ba, the ratio $j' = |J'/J|$ is of the order $10^{-3} - 10^{-4}$.

The study of the temperature dependence of the sublattice magnetization for quasi-2D antiferromagnets leads to an interesting non-analytic behaviour in a region

$\sqrt{JJ'} < k_BT < |J|$ in analogy with that found in the ferromagnetic case given by Eq. (2.5.15). For T lattices with $j' \ll 1$ well describing some of the HTCS, Eq. (7.4.23) becomes

$$\langle S_i^\zeta \rangle = S\left[1 - \frac{c'}{2S} - \frac{1}{2NS}\sum_{\boldsymbol{k}}\left(\sqrt{\frac{s_{\boldsymbol{k}}}{d_{\boldsymbol{k}}}} + \sqrt{\frac{d_{\boldsymbol{k}}}{s_{\boldsymbol{k}}}}\right) n_{\boldsymbol{k}}\right] \tag{7.4.27}$$

where $c' = 0.394$ is the value of the SQ lattice and

$$s_{\boldsymbol{k}} = \left[1 + \frac{1}{2}(\cos k_x + \cos k_y)\right] + \frac{1}{2}j'(1 + \cos k_z) \tag{7.4.28}$$

and

$$d_{\boldsymbol{k}} = \left[1 - \frac{1}{2}(\cos k_x + \cos k_y)\right] + \frac{1}{2}j'(1 - \cos k_z) \tag{7.4.29}$$

with k_x and k_y measured in units of in-plane lattice space a while k_z is measured in units of the out-of-plane distance c. For $k_BT < |J|$, the thermal contribution of Eq. (7.4.27) becomes

$$\begin{aligned}
\Delta M(T) &= \frac{1}{2NS}\sum_{\boldsymbol{k}}\left(\sqrt{\frac{s_{\boldsymbol{k}}}{d_{\boldsymbol{k}}}} + \sqrt{\frac{d_{\boldsymbol{k}}}{s_{\boldsymbol{k}}}}\right) n_{\boldsymbol{k}} \\
&\simeq \frac{1}{S(2\pi)^2}\int_{-\pi}^{\pi} dk_z \int_0^\infty k_\perp dk_\perp \left(\frac{1}{\epsilon_{\boldsymbol{k}}^-}\frac{1}{e^{\frac{8|J|S\epsilon_{\boldsymbol{k}}^-}{k_BT}} - 1} + \frac{1}{\epsilon_{\boldsymbol{k}}^+}\frac{1}{e^{\frac{8|J|S\epsilon_{\boldsymbol{k}}^+}{k_BT}} - 1}\right) \\
&= -\frac{1}{S(2\pi)^2}\frac{k_BT}{8|J|S}\int_{-\pi}^{\pi} dk_z \Big[\ln\left(1 - e^{-\frac{8|J|S}{k_BT}\sqrt{j'(1-\cos k_z)}}\right) \\
&\quad + \ln\left(1 - e^{-\frac{8|J|S}{k_BT}\sqrt{j'(1+\cos k_z)}}\right)\Big],
\end{aligned} \tag{7.4.30}$$

where $k_\perp^2 = k_x^2 + k_y^2$, $\epsilon_{\boldsymbol{k}}^\pm = \sqrt{k_\perp^2/2 + j'(1 \pm \cos k_z)}$. For $k_BT < \sqrt{JJ'}$, the exponential functions occurring in the arguments of the logarithmic functions in Eq. (7.4.30) can be replaced by their expansions around $k_z = 0$ (the first), and $k_z = \pi$ (the second one). Then the logarithmic functions so obtained can be expanded in their turn to give

$$\begin{aligned}
\Delta M(T) &= \frac{1}{S(2\pi)^2}\frac{k_BT}{8|J|S}4\sum_{n=1}^\infty \frac{1}{n}\int_0^\infty dk_z e^{-\frac{8|J|S}{k_BT}n\sqrt{\frac{j'}{2}}k_z} \\
&= \frac{\sqrt{2}\zeta(2)}{S\pi^2}\left(\frac{k_BT}{8|J|S}\right)^2 \frac{1}{\sqrt{j'}}.
\end{aligned} \tag{7.4.31}$$

Note the singular dependence on the coupling between planes j' which causes the thermal contribution to be orders of magnitude greater than for conventional 3D systems.

For $\sqrt{JJ'} < k_BT < |J|$, the exponential functions in Eq. (7.4.30) can be expanded in powers of their arguments obtaining

$$\Delta M(T) = -\frac{1}{S(2\pi)^2}\frac{k_BT}{8|J|S}2\int_0^\pi dk_z \ln\left[\left(\frac{8|J|S}{k_BT}\right)^2 j'\sin k_z\right]$$

$$= \frac{1}{2\pi S}\frac{k_BT}{8|J|S}\ln\left[\left(\frac{k_BT}{8|J|S}\right)^2\frac{2}{j'}\right]. \tag{7.4.32}$$

A new singular dependence on j' occurs at intermediate temperature. Equations (7.4.31) and (7.4.32) point out that at finite temperature the 2D antiferromagnet does not have LRO. However, any perturbation like the coupling between planes or easy-axis anisotropy in the plane restores the LRO.

7.5. Antiferromagnetism in Close-Packed Lattices

In the close-packed lattices like the triangular (TR), hexagonal (H), face centred cubic (FCC) and rhombohedral (R) lattice, the minimum of the classical energy (7.4.1) is no longer given by $\boldsymbol{Q}\cdot\boldsymbol{\delta} = \pi$. For instance, in the TR lattice, assuming a reference system in which the NNs are located at $\boldsymbol{\delta} = (\pm a, 0)$, $(\pm\frac{a}{2}, \pm\frac{\sqrt{3}}{2}a)$, the classical energy (7.4.1) becomes

$$E_0^{\mathrm{TR}} = 2|J|S^2N\left(\cos aQ_x + 2\cos\frac{aQ_x}{2}\cos\frac{\sqrt{3}}{2}aQ_y\right). \tag{7.5.1}$$

The absolute minimum has to be looked for among the simultaneous solutions of the two equations $\frac{\partial E_0}{\partial Q_x} = 0$ and $\frac{\partial E_0}{\partial Q_y} = 0$, that is

$$\sin\frac{aQ_x}{2}\left(2\cos\frac{aQ_x}{2} + \cos\frac{\sqrt{3}}{2}aQ_y\right) = 0 \tag{7.5.2}$$

and

$$\cos\frac{aQ_x}{2}\sin\frac{\sqrt{3}}{2}aQ_y = 0, \tag{7.5.3}$$

respectively. The solution of Eqs. (7.5.2) and (7.5.3) corresponding to the absolute minimum is

$$\boldsymbol{Q}^{\mathrm{TR}} = \left(\frac{4\pi}{3a}, 0\right) = \frac{1}{3}(\boldsymbol{a}^* + \boldsymbol{b}^*), \tag{7.5.4}$$

where

$$\boldsymbol{a}^* = \frac{2\pi}{a}\left(\mathbf{u}_x + \frac{1}{\sqrt{3}}\mathbf{u}_y\right), \quad \boldsymbol{b}^* = \frac{2\pi}{a}\left(\mathbf{u}_x - \frac{1}{\sqrt{3}}\mathbf{u}_y\right) \tag{7.5.5}$$

are the basic vectors of the reciprocal lattice. The energy (7.5.1) becomes

$$E_0^{\mathrm{TR}} = -3|J|S^2N. \tag{7.5.6}$$

The corresponding spin configuration is obtained from Eq. (7.3.13) where the generic lattice vector is given by

$$\boldsymbol{r}_{l,m} = \frac{a}{2}(l+m)\mathbf{u}_x + \frac{\sqrt{3}}{2}a(l-m)\mathbf{u}_y \tag{7.5.7}$$

with l, m integers. The spin vector localized at the site (l, m) is given by

$$\boldsymbol{S}_{l,m} = S\cos\left[\frac{2\pi}{3}(l+m)+\phi\right]\mathbf{u}_x + S\sin\left[\frac{2\pi}{3}(l+m)+\phi\right]\mathbf{u}_y. \tag{7.5.8}$$

From Eq. (7.5.8) one can see that the spins lie in the xy-plane and form a helix with a pitch of 120°. In Fig. 7.2, the ground-state configuration is shown for $\phi = 0$: the Néel antiferromagnetic configuration is not supported by the TR lattice. The physical reason is that if one supposes that two sublattices are antiparallel, *each* spin of the third sublattice could assume any direction since it is surrounded by three spins up and three spins down. For such a configuration the LRO is absent even at $T = 0$. This scenario is found in the TR Ising antiferromagnet where the scalar product of the Heisenberg Hamiltonian (7.1.1) is replaced by the product of the z-components of the spins. Indeed, Wannier[62] in 1950 showed that the TR Ising antiferromagnet has a *finite* entropy per spin at zero temperature $\frac{S(0)}{k_B N} = 0.5583$ and the LRO is absent even at $T = 0$. On the contrary, due to the rotation degree of freedom of the spins in the Heisenberg Hamiltonian (7.1.1), the minimum energy is realized by a spin configuration in which the spins of the three compenetrated sublattices rotate by an angle of 120° passing from one sublattice to the other and the LRO at $T = 0$ is recovered. The TR antiferromagnet is an example where the *frustration* by lattice structure prevents the Néel antiferromagnetic configuration. The same configuration characterizes the order in the triangular planes of the H lattice while the order along the c-axis is determined by the sign of the NN out-of-plane exchange interaction J': antiferromagnetic or ferromagnetic chains are obtained for $J' < 0$ or $J' > 0$, respectively. In the H lattice, the LRO is recovered at finite temperature by a mechanism similar to that seen in Eqs. (7.4.31) and (7.4.32).

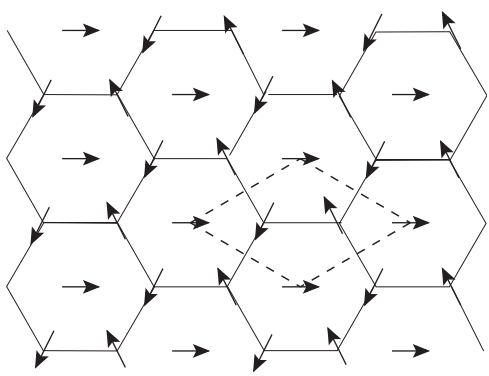

Fig. 7.2. Ground-state spin configuration for a TR antiferromagnet. The dashed line represents the magnetic unit cell.

The FCC lattice for which $\boldsymbol{\delta} = (\pm\frac{a}{2}, \pm\frac{a}{2}, 0)$, $(\pm\frac{a}{2}, 0, \pm\frac{a}{2})$ and $(0, \pm\frac{a}{2}, \pm\frac{a}{2})$ enters another type of frustration. The ground-state energy (7.4.1) becomes

$$E_0^{\rm FCC} = 4|J|S^2N\left(\cos\frac{aQ_x}{2}\cos\frac{aQ_y}{2} + \cos\frac{aQ_x}{2}\cos\frac{aQ_z}{2} + \cos\frac{aQ_y}{2}\cos\frac{aQ_z}{2}\right) \tag{7.5.9}$$

and the equations for the minimum $\frac{\partial E_0^{\rm FCC}}{\partial Q_i} = 0$ with $i = x, y, z$ become

$$\sin\frac{aQ_x}{2}\left(\cos\frac{aQ_y}{2} + \cos\frac{aQ_z}{2}\right) = 0, \tag{7.5.10}$$

$$\sin\frac{aQ_y}{2}\left(\cos\frac{aQ_x}{2} + \cos\frac{aQ_z}{2}\right) = 0 \tag{7.5.11}$$

and

$$\sin\frac{aQ_z}{2}\left(\cos\frac{aQ_x}{2} + \cos\frac{aQ_y}{2}\right) = 0. \tag{7.5.12}$$

In this case, the absolute minimum is no longer given by a unique wavevector or, more precisely, by the star of symmetric wavevectors that lead to the same spin configuration. In this case, the absolute minimum corresponds to an *infinite* continuous variety of wavevectors given by

$$\boldsymbol{Q}^{\rm FCC} = \left(\frac{2\pi}{a}\xi, 0, \frac{2\pi}{a}\right) = \frac{1}{2}\xi(\boldsymbol{a}^* + \boldsymbol{c}^*) + \frac{1}{2}(\boldsymbol{b}^* + \boldsymbol{c}^*), \tag{7.5.13}$$

where ξ is arbitrary and

$$\boldsymbol{a}^* = \frac{2\pi}{a}(\mathbf{u}_x + \mathbf{u}_y - \mathbf{u}_z), \quad \boldsymbol{b}^* = \frac{2\pi}{a}(\mathbf{u}_x - \mathbf{u}_y + \mathbf{u}_z), \quad \boldsymbol{c}^* = \frac{2\pi}{a}(-\mathbf{u}_x + \mathbf{u}_y + \mathbf{u}_z) \tag{7.5.14}$$

are the basic vectors of the reciprocal lattice. Obviously, the helix wavevectors obtained by cyclic permutations of Q_x, Q_y and Q_z lead to the same ground-state energy given by

$$E_0^{\rm FCC} = -4|J|S^2N. \tag{7.5.15}$$

Since Eq. (7.5.15) is independent of ξ, the classical ground-state energy of the FCC antiferromagnet is *infinitely* degenerate. Also the ground-state of the FCC Ising antiferromagnet[63] is highly degenerate ($2^{N^{1/3}}$) and LRO disappears even at $T = 0$. However, unlike the TR Ising antiferromagnet in the FCC Ising antiferromagnet the entropy per spin vanishes at $T = 0$.

The spin wave spectrum of the FCC Heisenberg antiferromagnet is obtained from Eqs. (7.3.10)–(7.3.12). Assuming to measure the lengths in units of the lattice

space a, one has

$$\hbar\omega_{\boldsymbol{k}} = 8|J|S\sqrt{s_{\boldsymbol{k}} d_{\boldsymbol{k}}} \tag{7.5.16}$$

where

$$s_{\boldsymbol{k}} = 1 + \cos x \cos y + \cos x \cos z + \cos y \cos z \tag{7.5.17}$$

and

$$d_{\boldsymbol{k}} = 1 - \cos y \cos z + \cos(\pi\xi)\cos x\,(\cos y - \cos z) \tag{7.5.18}$$

with $x = \frac{ak_x}{2}$, $y = \frac{ak_y}{2}$ and $z = \frac{ak_z}{2}$. As one can see from Eq. (7.5.18), the spin wave spectrum has a line of soft modes corresponding to the x-axis ($k_y = k_z = 0$). The presence of a *soft line* in the spin wave spectrum causes the divergence of the third term of Eq. (7.3.14) pointing out that the LRO is absent at any finite temperature. It is interesting to understand how the classical scenario is modified when quantum fluctuations are taken into account. To this end, we evaluate the first quantum correction to the classical ground-state energy given by Eq. (7.2.16). For the FCC lattice one obtains

$$\Delta E_0^{\rm FCC} = 4|J|SN[I^{\rm FCC}(\xi) - 1] \tag{7.5.19}$$

where

$$I^{\rm FCC}(\xi) = \frac{1}{\pi^3}\int_0^\pi dx \int_0^\pi dy \int_0^\pi dz \sqrt{s_{\boldsymbol{k}} d_{\boldsymbol{k}}}\ . \tag{7.5.20}$$

As one can see from Eqs. (7.5.20), (7.5.17) and (7.5.18), the first quantum correction to the classical ground state is a function of ξ through the term $d_{\boldsymbol{k}}$ appearing in the spin wave spectrum. The minimum of the first-order ground-state energy corresponds to the minimum of $I^{\rm FCC}(\xi)$ and the ground-state configuration is obtained replacing the value of ξ that minimizes $I^{\rm FCC}(\xi)$ into Eq. (7.5.13). A numerical evaluation of the integral (7.5.20) shows that $I^{\rm FCC}(\xi)$ is minimum for $\xi = 0$ and $\xi = 1$ [$I^{\rm FCC}(0) = I^{\rm FCC}(1) = 0.75584$] and maximum for $\xi = \frac{1}{2}$ [$I^{\rm FCC}(\frac{1}{2}) = 0.79661$]. Consequently, the zero-point energy has the absolute minimum at $Q_x = 0$ and $Q_x = \frac{2\pi}{a}$. The corresponding helix wavevectors become

$$\boldsymbol{Q}_{\rm GS}^{\rm FCC} = \left(0, 0, \frac{2\pi}{a}\right) \quad \text{and} \quad \boldsymbol{Q}_{\rm GS}^{\rm FCC} = \left(\frac{2\pi}{a}, 0, \frac{2\pi}{a}\right). \tag{7.5.21}$$

From the generic vector of the FCC lattice

$$\boldsymbol{r}_{l,m,n} = \frac{a}{2}(l+m)\mathbf{u}_x + \frac{a}{2}(l+n)\mathbf{u}_y + \frac{a}{2}(m+n)\mathbf{u}_z \tag{7.5.22}$$

with l, m, n integers and from the first helix wavevector of Eq. (7.5.21), one obtains the ground-state configuration of the FCC lattice

$$\boldsymbol{S}_{l,m,n} = S\cos[\pi(m+n)+\phi]\mathbf{u}_x + S\sin[\pi(m+n)+\phi]\mathbf{u}_y. \tag{7.5.23}$$

This configuration corresponds to a stacking of alternating ferromagnetic planes perpendicular to the z-axis as shown in Fig. 7.3. This kind of antiferromagnetic order is classified as "antiferromagnetic order of type AF1". From the second helix

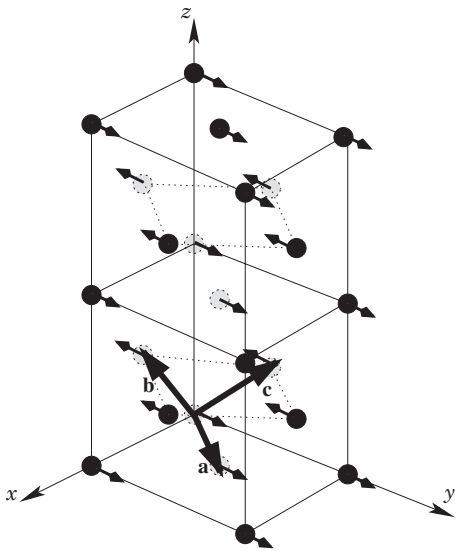

Fig. 7.3. FCC antiferromagnet. Ground-state configuration obtained accounting for the first-order quantum correction. The thick arrows represent the basic lattice vectors of the FCC lattice.

wavevector of Eq. (7.5.21), one obtains a ground-state configuration similar to the previous one. The only difference is that the ferromagnetic planes are perpendicular to the y-axis. From Eq. (7.5.23), one sees that the spins make an angle ϕ (arbitrary) with the x-axis even though the configuration shown in Fig. 7.3 corresponds to the choice $\phi = \frac{\pi}{2}$. The fact that the spins lie in the xy-plane is due to the broken symmetry entered by the initial choice of the cone axis parallel to the z-axis. In other words, the calculations performed in this chapter are reminiscent of a single-ion easy-plane anisotropy $D \to 0^+$. Physically, only the anisotropy entered by the crystal field can select the angles θ and ϕ in actual compounds. For a configuration as shown in Fig. 7.3, the lattice anisotropy is expected to choose between the high symmetry values $\phi = 0$ (1,0,0), [or $\phi = \frac{\pi}{2}$ (0,1,0)] and $\phi = \frac{\pi}{4}$ (1,1,0) according to x (y) are easy-axis or a hard-axis. The antiferromagnetic order of type AF1 was observed in UO_2 by neutron-diffraction[64] below $T_N \simeq 31\,\mathrm{K}$. The magnetic uranium ions U^{4+} are located on the nodes of a FCC lattice and their magnetic moments ($\sim 1.8\mu_B$) lie within the alternating ferromagnetic sheets: the orientation of the antiferromagnetic axis in the xy-plane could not be singled out, however, because of the multidomain structure of the sample.

We have seen that in the FCC antiferromagnet the quantum fluctuations destroy the infinite degeneracy present in classic approximation, leading to an ordered ground state. This fact is referred as *order by quantum disorder*.[65] Another interesting question is about the thermal contribution to the free energy as given by the temperature-dependent term of Eq. (7.4.13). Since the spin wave spectrum is a function of ξ through $d_{\boldsymbol{k}}$ given by Eq. (7.5.18), the question is: which helix wavevectors are selected by thermal fluctuations? A numerical evaluation of the

temperature-dependent integral (7.4.13) shows that it has a minimum at $\xi = 0$ and a maximum at $\xi = \frac{1}{2}$ so that also thermal fluctuations select the helix wavevector of the quantum ground state. This means that at increasing temperature, a change of the helix wavevector is not expected. The selection of a helix wavevector by thermal fluctuations is called *order by thermal disorder*.[66] Similar results are obtained for the R lattice[66] shown in Fig. 7.4. Notice that solid oxygen between 24 and 44 K shows a phase known as β-oxygen with the rhombohedral structure and direct exchange interaction between the O_2 molecules.[67] With the choice of axes shown in Fig. 7.4, the energy (7.4.1) becomes

$$\begin{aligned} E_0^{\mathrm{R}} = {} & 2|J|S^2N\left(\cos aQ_y + 2\cos\frac{\sqrt{3}}{2}aQ_x\cos\frac{aQ_y}{2}\right) \\ & -2J'S^2N\left[\cos\frac{cQ_z}{3}\left(\cos\frac{aQ_x}{\sqrt{3}} + 2\cos\frac{aQ_x}{2\sqrt{3}}\cos\frac{aQ_y}{2}\right)\right. \\ & \left. +\sin\frac{cQ_z}{3}\left(\sin\frac{aQ_x}{\sqrt{3}} - 2\sin\frac{aQ_x}{2\sqrt{3}}\cos\frac{aQ_y}{2}\right)\right], \end{aligned} \tag{7.5.24}$$

where $J < 0$ and J' are the exchange integrals between the NN in the plane and out-of-plane, respectively (Fig. 7.4). Defining the following quantities

$$e_0 = \frac{E_0^{\mathrm{R}}}{6|J|S^2N}, \quad x_0 = \frac{\sqrt{3}}{2}aQ_x, \quad y_0 = \frac{aQ_y}{2}, \quad z_0 = \frac{cQ_z}{3}, \quad j' = \frac{J'}{|J|}, \tag{7.5.25}$$

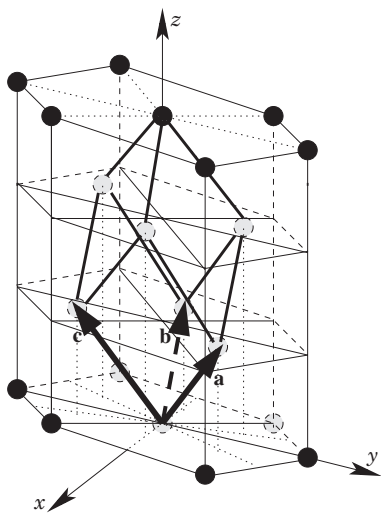

Fig. 7.4. Rhombohedral lattice with the lattice vectors of the primitive cell.

Equation (7.5.24) becomes

$$e_0 = \frac{1}{3}\Bigg\{\cos 2y_0 + 2\cos x_0 \cos y_0 - j'\Bigg[\cos z_0\left(\cos\frac{2x_0}{3} + 2\cos\frac{x_0}{3}\cos y_0\right) + \sin z_0\left(\sin\frac{2x_0}{3} - 2\sin\frac{x_0}{3}\cos y_0\right)\Bigg]\Bigg\}. \quad (7.5.26)$$

The minimum conditions $\frac{\partial e_0}{\partial x_0} = 0$, $\frac{\partial e_0}{\partial y_0} = 0$ and $\frac{\partial e_0}{\partial z_0} = 0$ lead to the equations

$$\sin x_0 \cos y_0\left(1 - \frac{j'\cos z_0}{\cos\frac{2x_0}{3} + 2\cos\frac{x_0}{3}\cos y_0}\right) = 0, \quad (7.5.27)$$

$$\sin y_0\,(2\cos y_0 + \cos x_0)\left(1 - \frac{j'\cos z_0}{\cos\frac{2x_0}{3} + 2\cos\frac{x_0}{3}\cos y_0}\right) = 0 \quad (7.5.28)$$

and

$$\tan z_0 = \frac{2\sin\frac{x_0}{3}\left(\cos\frac{x_0}{3} - \cos y_0\right)}{\cos\frac{2x_0}{3} + 2\cos\frac{x_0}{3}\cos y_0}, \quad (7.5.29)$$

respectively. Using the trigonometric relationship

$$\cos z_0 = \pm\frac{1}{\sqrt{1+\tan^2 z_0}},$$

Eqs. (7.5.26)–(7.5.28) become

$$\sin x_0 \cos y_0\left(1 - \frac{|j'|}{\sqrt{1 + 4\cos x_0\cos y_0 + 4\cos^2 y_0}}\right) = 0, \quad (7.5.30)$$

$$\sin y_0\,(2\cos y_0 + \cos x_0)\left(1 - \frac{|j'|}{\sqrt{1 + 4\cos x_0\cos y_0 + 4\cos^2 y_0}}\right) = 0 \quad (7.5.31)$$

and

$$\cos z_0 = \pm\frac{\cos\frac{2x_0}{3} + 2\cos\frac{x_0}{3}\cos y_0}{\sqrt{1 + 4\cos x_0\cos y_0 + 4\cos^2 y_0}} \quad (7.5.32)$$

with

$$e_0 = \frac{1}{3}\Big(\cos 2y_0 + 2\cos x_0\cos y_0 - |j'|\sqrt{1 + 4\cos x_0\cos y_0 + 4\cos^2 y_0}\Big). \quad (7.5.33)$$

The upper and lower signs in Eq. (7.5.32) correspond to $j' > 0$ (ferromagnetic out-of-plane exchange interaction) and $j' < 0$ (antiferromagnetic out-of-plane exchange interaction), respectively. Notice that Eqs. (7.5.30), (7.5.31) and (7.5.33) are independent of the sign of j' while the sign of j' is important in Eq. (7.5.32) that is crucial to obtain the configuration corresponding to the minimum energy. The absolute minimum of the classical energy corresponds to

$$x_0 = 0, \quad y_0 = 0, \quad e_0 = 1 - |j'| \quad (7.5.34)$$

with $z_0 = \pi$ or 0 for $j' < -3$ or $j' > 3$, respectively. For $-3 \leq j' \leq 3$, the minimum is no longer an *isolated point* but it consists of a *continuous line* given by the vanishing of the common term in Eqs. (7.5.30) and (7.5.31), that is,

$$4\cos^2\frac{Q_y}{2} + 4\cos\frac{\sqrt{3}}{2}Q_x\cos\frac{Q_y}{2} + 1 - j'^2 = 0. \tag{7.5.35}$$

The corresponding Q_z is given by the equation

$$\cos\frac{Q_z}{3} = \frac{1}{j'}\left(\cos\frac{Q_x}{\sqrt{3}} + 2\cos\frac{Q_x}{2\sqrt{3}}\cos\frac{Q_y}{2}\right), \tag{7.5.36}$$

where Q_x and Q_y are solutions of Eq. (7.5.35). The corresponding classical energy is given by

$$e_0 = -\frac{1}{2} - \frac{1}{6}j'^2. \tag{7.5.37}$$

This infinitely degenerate minimum in the classical energy leads to a *degenerate helix* (DH).[66] The DH given by Eq. (7.5.35) is shown in Fig. 7.5 for $0 < |j'| < 1$ and in Fig. 7.6 for $1 < |j'| < 3$. Notice that the projection of the DH line onto the Q_xQ_y-plane is invariant under the change of sign of j' as shown by the left panels of Figs. 7.5 and 7.6 while the projection onto the Q_xQ_z-plane is reversed by the change of sign of j': compare the central ($j' > 0$) with the panel on the right ($j' < 0$) of Figs. 7.5 and 7.6. The curve (7.5.35) reduces to a circle of equation

$$Q_x^2 + \left(Q_y - \frac{4\pi}{3}\right)^2 = \frac{4}{3}j'^2 \tag{7.5.38}$$

for $|j'| \to 0$ and to a circle of equation

$$Q_x^2 + Q_y^2 = \frac{2}{3}(9 - j'^2) \tag{7.5.39}$$

for $|j'| \to 3$. For $|j'| = 0$ and $|j'| = 3$, Eqs. (7.5.38) and (7.5.39) reduce to the points $(0, \frac{4\pi}{3})$ and $(0, 0)$, respectively. For $|j'| \to 1^-$, the curve given by Eq. (7.5.35) reduces to an equilateral triangle with barycentre in $(0, \frac{4\pi}{3})$ while for $|j'| \to 1^+$, the curve given by Eq. (7.5.35) reduces to a hexagon centred in the origin.

7.6. Order by Quantum and Thermal Disorder

In the previous section, we have seen that a R lattice shows an infinite degeneracy in the (classical) ground state for $|J'/J| < 3$. In this section, we will see how the quantum and thermal fluctuations destroy this infinite degeneracy. This can be done evaluating explicitly the free energy (7.4.13) for the R lattice assuming that the helix wavevector belongs to the DH given by Eqs. (7.5.35) and (7.5.36). By use

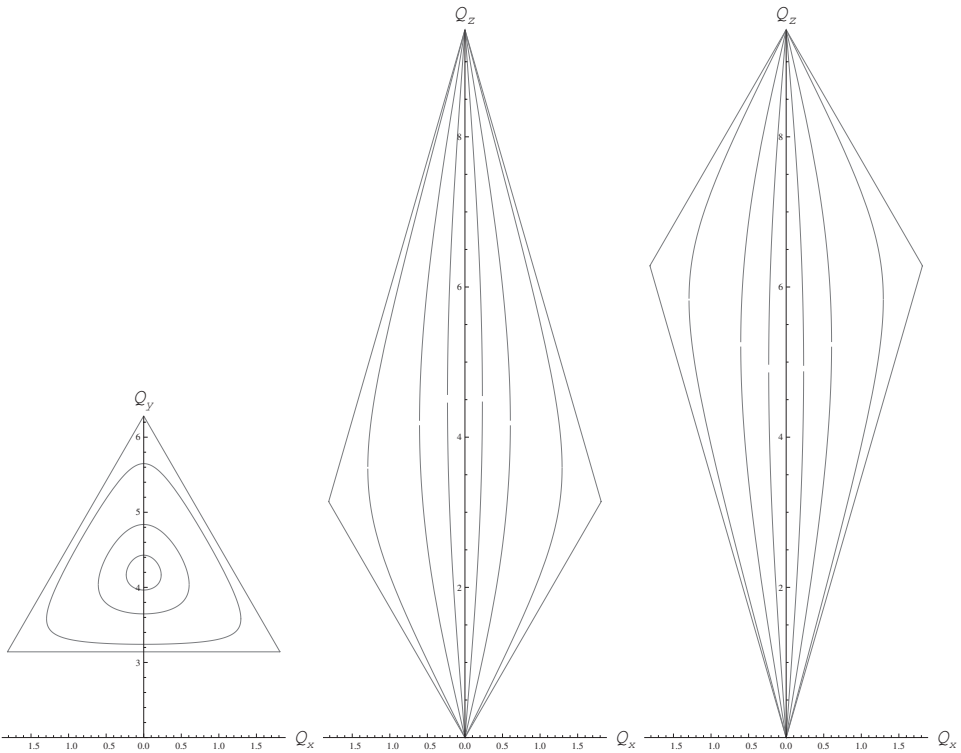

Fig. 7.5. DH of the rhombohedral antiferromagnet for $0 < |j'| < 1$. Left panel: The projection onto the Q_xQ_y-plane of the DH line for $|j'| = 0.2, 0.5, 0.9, 1^-$ going from the inner to the outer curve. Central panel: The projection onto the Q_xQ_z-plane of the DH line for $j' = 0.2, 0.5, 0.9, 1^-$ going from the inner to the outer curve. Right panel: The projection onto the Q_xQ_z-plane of the DH line for $j' = -0.2, -0.5, -0.9, -1^-$ going from the inner to the outer curve.

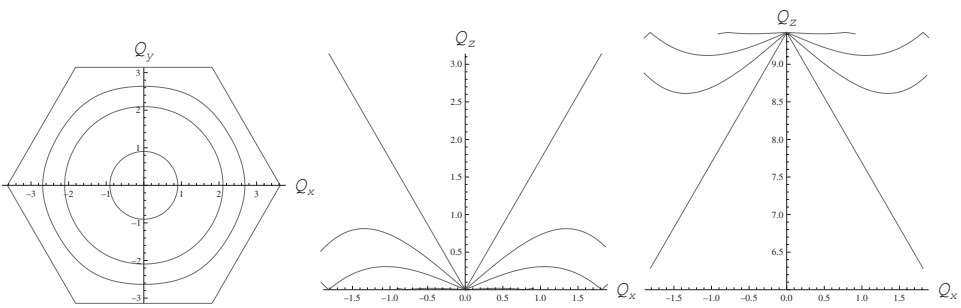

Fig. 7.6. DH of the rhombohedral antiferromagnet for several $1 < |j'| < 3$. Left panel: The projection onto the Q_xQ_y-plane of the DH line for $|j'| = 2.8, 2, 1.5, 1^+$ going from the inner to the outer curve. Central panel: The projection onto the Q_xQ_z-plane of the DH line for $j' = 2.8, 2, 1.5, 1^+$ going from the lowest to the highest curve. Right panel: The projection onto the Q_xQ_z-plane of the DH line for $j' = -2.8, -2, -1.5, -1^+$ going from the highest to the lowest curve.

of Eqs. (7.2.16) and (7.5.37) the ground-state energy becomes

$$E_{\rm GS} = E_0 - \frac{1}{2}\sum_{\boldsymbol{k}} A_{\boldsymbol{k}}^{(\rm s)} + \frac{1}{2}\sum_{\boldsymbol{k}} \hbar\omega_{\boldsymbol{k}}$$

$$= -3|J|S^2N\left(1+\frac{1}{3}j'^2\right)\left(1+\frac{1}{S}\right) + 2|J|SN\Delta, \tag{7.6.1}$$

where

$$\Delta = \frac{1}{2(2\pi)^3}\int_{-2\pi}^{2\pi} dx \int_{-\pi}^{\pi} dy \int_{0}^{2\pi} dz \sqrt{s(x,y,z)d_{\boldsymbol{Q}}(x,y,z)} \tag{7.6.2}$$

with

$$s(x,y,z) = \frac{3}{2} + \frac{1}{2}j'^2 + 2\cos x\cos y + \cos 2y - j'\cos z\left(2\cos\frac{x}{3}\cos y + \cos\frac{2x}{3}\right)$$

$$- j'\cos z\left(2\cos\frac{x}{3}\cos y + \cos\frac{2x}{3}\right) - 2j'\sin z\sin\frac{x}{3}\left(\cos\frac{x}{3} - \cos y\right) \tag{7.6.3}$$

and

$$d_{\boldsymbol{Q}}(x,y,z) = -2\cos x_0\cos y_0(1-\cos x\cos y) - \cos 2y_0(1-\cos 2y) + 2\sin x_0\sin y_0$$

$$\times \sin x\sin y + 2j'\cos\left(\frac{x_0}{3}+z_0\right)\cos y_0\left[1-\cos\left(\frac{x}{3}+z\right)\cos y\right]$$

$$- 2j'\sin\left(\frac{x_0}{3}+z_0\right)\sin y_0\sin\left(\frac{x}{3}+z\right)\sin y$$

$$+ j'\cos\left(\frac{2x_0}{3}-z_0\right)\left[1-\cos\left(\frac{2x}{3}-z\right)\right]. \tag{7.6.4}$$

In Eqs. (7.6.3) and (7.6.4), x, y, z mean $x = \frac{\sqrt{3}}{2}ak_x$, $y = \frac{1}{2}ak_y$ and $z = \frac{1}{3}ck_z$. Notice that $s(x,y,z)$ is independent of $\boldsymbol{Q}$ ($x_0 = \frac{\sqrt{3}}{2}aQ_x$, $y_0 = \frac{1}{2}aQ_y$ and $z_0 = \frac{1}{3}cQ_z$). The only $\boldsymbol{Q}$ dependence of the spin wave spectrum comes from $d_{\boldsymbol{Q}}(x,y,z)$. The integration is performed using a tetragonal cell containing four primitive rhombohedral cells. The numerical integration leads to the functions Δ shown in Fig. 7.7 for $j' = 0.9, 0.8, 0.5$ (left panel) and $j' = -0.9, -0.8, -0.5$ (right panel). Notice that for ferromagnetic coupling between planes along the c-axis ($j' > 0$), the zero-point motion is a periodic function of Q_z of period $\frac{2\pi}{c}$ while for antiferromagnetic coupling between the planes ($j' < 0$) Δ is a periodic function of Q_z with a period $\frac{6\pi}{c}$. Moreover, for $j' > 0$, one can see that the minimum of Δ corresponds to $Q_z = \frac{\pi}{c}$ for any j', while for $j' < 0$, the minimum of Δ corresponds to a helix wavevector which is a function of j'. In any case, Fig. 7.7 illustrates what is the meaning of *order by quantum disorder* since it is the first quantum correction to the classical ground state that selects the helix wavevector of the ground-state configuration through the integral over the spin wave spectrum.

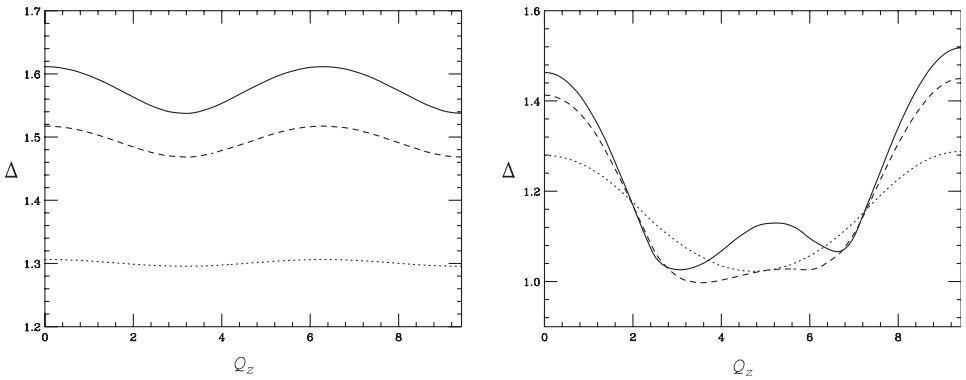

Fig. 7.7. First quantum correction to the ground-state energy of a rhombohedral lattice as function of Q_z moving along the DH helix. Left panel: $j' = 0.9$ (continuous curve), $j' = 0.8$ (dashed curve) and $j' = 0.5$ (dotted curve). Right panel: $j' = -0.9$ (continuous curve), $j' = -0.8$ (dashed curve) and $j' = -0.5$ (dotted curve).

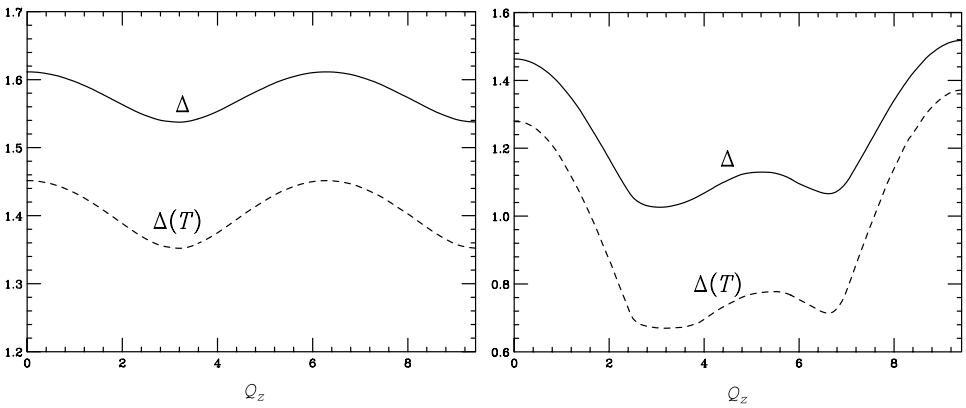

Fig. 7.8. Free energy as function of Q_z moving along the DH line for $T = 0$ (continuous curves) and $\frac{k_B T}{4|J|S} = 0.5$ (dashed curves). Left panel: $j' = 0.9$. Right panel: $j' = -0.9$.

The free energy of the R lattice in the harmonic approximation reads

$$F = E_{\rm GS} + k_B T \sum_{\boldsymbol{k}} \ln(1 - e^{-\beta\hbar\omega_{\boldsymbol{k}}})$$

$$= -3|J|S^2 N \left(1 + \frac{1}{3} j'^2\right)\left(1 + \frac{1}{S}\right) + 2|J|SN\Delta(T), \tag{7.6.5}$$

where

$$\Delta(T) = \Delta + \frac{\tau}{(2\pi)^3} \int_{-2\pi}^{2\pi} dx \int_{-\pi}^{\pi} dy \int_{0}^{2\pi} dz \ \ln\left(1 - e^{-\frac{1}{\tau}\sqrt{s(x,y,z) d_{\boldsymbol{Q}}(x,y,z)}}\right), \tag{7.6.6}$$

with $\tau = \frac{k_B T}{4|J|S}$ and Δ given by Eq. (7.6.2). The numerical integration of Eq. (7.6.6) is shown in Fig. 7.8 for $j' = \pm 0.9$ and $\tau = 0.5$ (dashed curves). For comparison,

the corresponding curves at $T = 0$ (continuous curves) are shown in the same figure. The dashed curves illustrate the meaning of *order by thermal disorder*. Indeed, in this case the thermal fluctuations select the helix wavevector of the minimum of $\Delta(T)$. Within the numerical accuracy, the minima at finite temperature are not distinct from those at zero temperature so that no evidence of temperature dependence of the helix wavevector $\boldsymbol{Q}$ is found.

7.7. Frustration by Competing Interactions: Square Lattice

In this section, we study another kind of frustration entered by the competing exchange interactions.

The ground-state energy of a SQ lattice with exchange interactions up to TNN is given by

$$E_0^{\mathrm{SQ}} = 4J_1 S^2 N e_0 \tag{7.7.1}$$

where $J_1 > 0$ and

$$e_0 = -\gamma_{\boldsymbol{Q}}^{(1)} - j_2\gamma_{\boldsymbol{Q}}^{(2)} - j_3\gamma_{\boldsymbol{Q}}^{(3)} \tag{7.7.2}$$

with

$$\gamma_{\boldsymbol{Q}}^{(1)} = \frac{1}{2}(\cos x_0 + \cos y_0), \tag{7.7.3}$$

$$\gamma_{\boldsymbol{Q}}^{(2)} = \cos x_0 \cos y_0, \tag{7.7.4}$$

$$\gamma_{\boldsymbol{Q}}^{(3)} = \frac{1}{2}(\cos 2x_0 + \cos 2y_0) \tag{7.7.5}$$

and

$$x_0 = aQ_x, \quad y_0 = aQ_y, \quad j_\alpha = \frac{J_\alpha}{J_1}. \tag{7.7.6}$$

The minimum conditions are given by

$$\sin x_0(1 + 2j_2 \cos y_0 + 4j_3 \cos x_0) = 0, \tag{7.7.7}$$

$$\sin y_0(1 + 2j_2 \cos x_0 + 4j_3 \cos y_0) = 0. \tag{7.7.8}$$

The minimum configurations in the j_2j_3-plane are illustrated in Fig. 7.9. The j_2j_3-plane is divided in four regions and the corresponding energies and helix wavevectors are given by

F: ferromagnetic phase

$$x_0 = y_0 = 0, \quad e_0^{\mathrm{F}} = -1 - j_2 - j_3. \tag{7.7.9}$$

$\mathbf{AF_1}$: antiferromagnetic collinear order in which the spins along the $(1, 0)$ lines are parallel

$$x_0 = 0, \quad y_0 = \pi, \quad e_0^{\mathrm{AF}_1} = j_2 - j_3. \tag{7.7.10}$$

Obviously, the symmetric phase with $x_0 = \pi$ and $y_0 = 0$ in which the parallel spins are along the $(0, 1)$ lines are degenerate with Eq. (7.7.10).

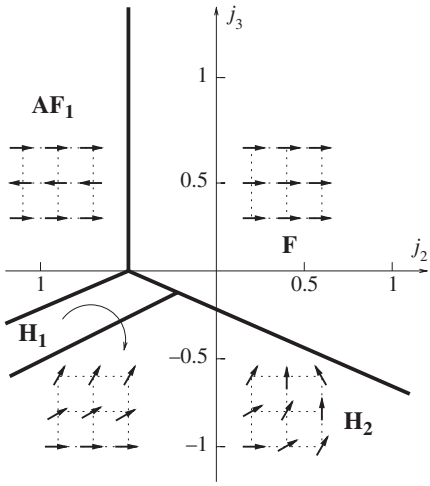

Fig. 7.9. Ground-state configurations of a SQ lattice with competing interactions $j_\alpha = \frac{J_\alpha}{J_1}$ and $J_1 > 0$.

$\mathbf{H_1}$: non-collinear order in which the spins are parallel along the $(1,0)$ direction and make an angle y_0 moving along the $(0,1)$ direction

$$x_0 = 0, \quad y_0 = \arccos\left(-\frac{1+2j_2}{4j_3}\right), \quad e_0^{\mathrm{H}_1} = -\frac{1}{2} + \frac{(1+2j_2)^2}{16j_3}. \tag{7.7.11}$$

The same energy is obtained by exchanging x_0 and y_0. In this case, the spins are parallel along the $(0,1)$ direction and make an angle x_0 along the $(1,0)$ direction. In general, this magnetic order is *incommensurate* with the lattice periodicity.

$\mathbf{H_2}$: non-collinear order in which the spins are parallel along the $(1,-1)$ direction and make an angle x_0 moving along the $(1,1)$ direction

$$x_0 = y_0 = \arccos\left[-\frac{1}{2(j_2+2j_3)}\right], \quad e_0^{\mathrm{H}_2} = j_3 + \frac{1}{4(j_2+2j_3)}. \tag{7.7.12}$$

Obviously, another energy minimum exists for $x_0 = -y_0$. In this case, the parallel spins are along the $(1,1)$ direction and make an angle x_0 along the $(1,-1)$ direction.

The boundaries between the different regions shown in Fig. 7.9 are lines of continuous (second order) phase transitions except the lines between regions $\mathbf{AF}_1 - \mathbf{F}$ where the transition is first order and $\mathbf{H_1} - \mathbf{H_2}$ which is a *disorder* line. The equations of the separation lines between the different regions are

$\mathbf{AF_1} - \mathbf{F} : j_2 = -\frac{1}{2}$,
$\mathbf{F} - \mathbf{H_1}$ and $\mathbf{F} - \mathbf{H_2} : j_3 = -\frac{1}{4}(1+2j_2)$,
$\mathbf{AF_1} - \mathbf{H_1} : j_3 = \frac{1}{4}(1+2j_2)$,
$\mathbf{H_1} - \mathbf{H_2} : j_3 = \frac{1}{2}j_2$.

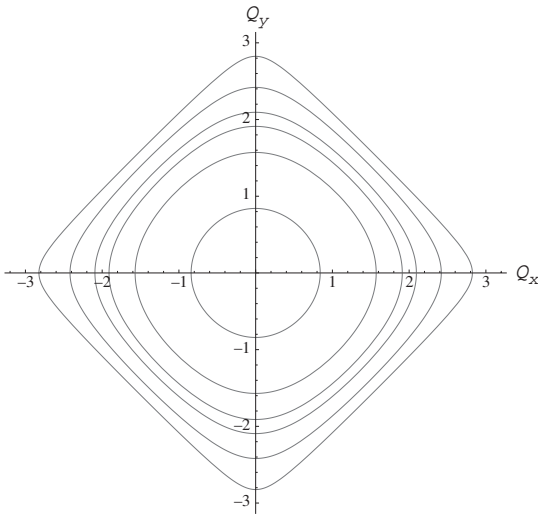

Fig. 7.10. Infinite degeneration line of the SQ lattice in the reciprocal space for several j_2 ($j_3 = \frac{1}{2}j_2$). From the inner to the outer curve: $j_2 = -0.3$, -0.5, -0.75, -1, -2, -10, respectively.

Notice that for $j_3 = \frac{1}{2}j_2$ Eqs. (7.7.7) and (7.7.8) are simultaneously satisfied assuming

$$\cos x_0 + \cos y_0 = -\frac{1}{2j_2} \tag{7.7.13}$$

so that the minima form a line in the reciprocal space given by

$$Q_y = \arccos\left(-\frac{1}{2j_2} - \cos Q_x\right) \tag{7.7.14}$$

with an infinitely degenerate ground-state energy given by

$$e_0^{\mathrm{DH}} = \frac{1}{2}j_2 + \frac{1}{8j_2}. \tag{7.7.15}$$

The DH given by Eq. (7.7.14) is shown in Fig. 7.10 for $j_2 = -0.3, -0.5, -0.75, -1, -2, -10$ going from the inner to the outer curve. Notice that for $j_2 = -0.25$, the DH shrinks to the point (0,0), and for $j_2 \to \infty$, it becomes a square given by $Q_y = \pm(\pi - |Q_x|)$ with $-\pi < Q_x < \pi$. The infinite degeneracy of the ground state implies absence of LRO even at $T = 0$. This infinite degeneracy, however, is destroyed by quantum fluctuations or by the addition of interactions to spins further. Indeed, the first quantum correction to the classical ground state is given by

$$E_{\mathrm{GS}}^{\mathrm{DH}} = 4J_1S^2N\left[\left(\frac{1}{2}j_2 + \frac{1}{8j_2}\right)\left(1 + \frac{1}{S}\right) + \frac{\Delta}{S}\right], \tag{7.7.16}$$

where

$$\Delta = \frac{1}{(2\pi)^2}\int_{-\pi}^{\pi} dx \int_{-\pi}^{\pi} dy \sqrt{s(x,y)d_{\boldsymbol{Q}}(x,y)} \tag{7.7.17}$$

with

$$s(x,y) = -\frac{1}{2}j_2 - \frac{1}{8j_2} - \frac{1}{2}(\cos x + \cos y) - j_2 \cos x \cos y - \frac{j_2}{4}(\cos 2x + \cos 2y), \tag{7.7.18}$$

$$d_{\boldsymbol{Q}}(x,y) = \frac{1}{2}[\cos x_0(1-\cos x) + \cos y_0(1-\cos y)] + j_2 \cos x_0 \cos y_0 \times (1 - \cos x \cos y) - j_2 \sin x_0 \sin y_0 \sin x \sin y + \frac{j_2}{4}[(\cos 2x_0)(1-\cos 2x) + \cos 2y_0(1-\cos 2y)] \tag{7.7.19}$$

and

$$y_0 = \arccos\left(-\frac{1}{2j_2} - \cos x_0\right). \tag{7.7.20}$$

The numerical evaluation of the 2D integral in Eq. (7.7.17) shows that the minima of Δ occur at $x_0 = 0$, $y_0 = \arccos(-\frac{1}{2j_2} - 1)$ and $x_0 = \arccos(-\frac{1}{2j_2} - 1)$, $y_0 = 0$ corresponding to the helix $\mathbf{H_1}$ while the maxima of Δ are located at $x_0 = \pm y_0$ where $x_0 = \arccos(-\frac{1}{4j_2})$ corresponding to the helix $\mathbf{H_2}$. This result points out that the disorder line $j_3 = \frac{1}{2}j_2$ becomes a first-order transition line between the $\mathbf{H_1}$ and $\mathbf{H_2}$ phases. More precisely, the existence region of the helix $\mathbf{H_1}$ shown in Fig. 7.9 is expected to widen at the expense of the existence region of the helix $\mathbf{H_2}$ since the gap between the energies of the helices $\mathbf{H_2}$ and $\mathbf{H_1}$ increases with $|j_2|$. The LRO at $T = 0$ is recovered on the "new" boundary line $\mathbf{H_1} - \mathbf{H_2}$ which becomes a first-order transition line. One can say that the first-order transition between the phases $\mathbf{H_1}$ and $\mathbf{H_2}$ is driven by quantum fluctuations.

A similar effect is obtained introducing a fourth nearest neighbour (FNN) exchange interaction $j_4 = \frac{2J_4}{J_1}$ in the classical ground-state energy. Indeed, j_4 does not change the qualitative feature of the phase diagram of Fig. 7.9. The main change is the disappearance of the disorder line between the helices $\mathbf{H_1}$ and $\mathbf{H_2}$ replaced by a first-order transition line. The quantitative effect of the FNN interaction is to shift the boundary lines as shown in Fig. 7.11 for $j_4 = 0.1$ (a) and $j_4 = -0.1$ (b), respectively. The thin lines in both figures correspond to the case $j_4 = 0$ shown in Fig. 7.9. The points $\mathrm{P}_1(-0.475, -0.1375)$ and $\mathrm{P}_2(-0.025, -0.1125)$ are triple points where two second-order transition lines and one first-order transition line meet.

The phase diagram at $T = 0$ of the T lattice with competing interactions in the xy-plane is the same as that shown in Figs. 7.9 and 7.11. Indeed, the ground-state energy of the T lattice may be obtained from the SQ energy (7.7.2) by the simple addition of the out-of-plane interaction term $j'\gamma'_{\boldsymbol{Q}}$ with $j' = J'/J_1$ and $\gamma'_{\boldsymbol{Q}} = \cos z_0$ ($z_0 = cQ_z$). The stacking of planes along the (0,0,1) is ordered ferromagnetically ($z_0 = 0$) or antiferromagnetically ($z_0 = \pi$) according to $j' > 0$ or $j' < 0$, respectively. For the T lattice, the presence of the disorder line $j_3 = \frac{1}{2}j_2$ implies the absence of LRO at any finite temperature.

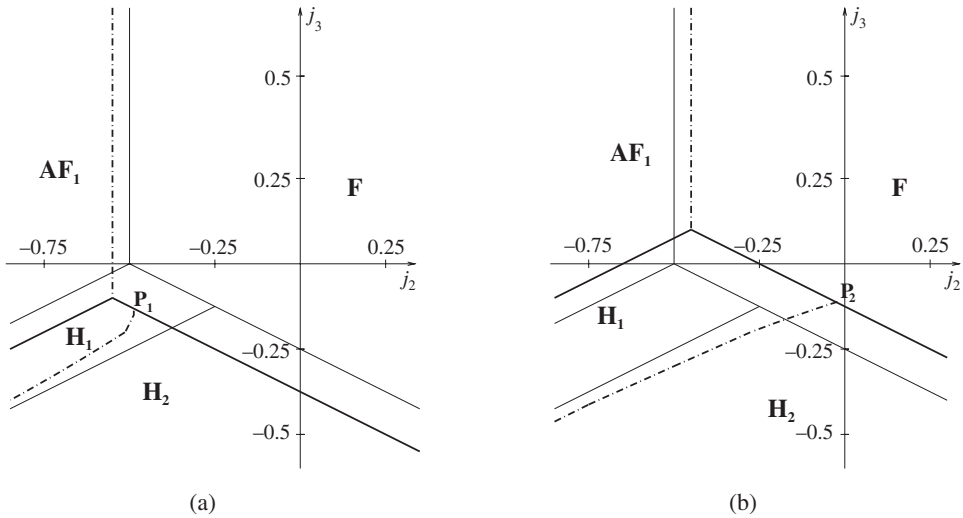

Fig. 7.11. Ground-state configurations of a SQ lattice with competing interactions $j_\alpha = \frac{z_\alpha J_\alpha}{z_1 J_1}$ and $J_1 > 0$: thick lines (a) $j_4 = 0.1$; (b) $j_4 = -0.1$; thin lines $j_4 = 0$. The dashed lines mean first-order transition lines.

For $J_1 < 0$, the classical ground-state energy of the SQ lattice becomes

$$E_0^{\rm SQ} = 4|J_1|S^2 N e_0 \tag{7.7.21}$$

where

$$e_0 = \gamma_{\boldsymbol{Q}}^{(1)} + j_2\gamma_{\boldsymbol{Q}}^{(2)} + j_3\gamma_{\boldsymbol{Q}}^{(3)}. \tag{7.7.22}$$

Notice that from the definition $j_\alpha = J_\alpha/J_1$ with $\alpha = 2, 3$, the positive j_α correspond to both J_α and J_1 antiferromagnetic interactions. The phase diagram at $T = 0$ is shown in Fig. 7.12. The $j_2 j_3$-plane is divided in four regions whose helix wavevectors and energies are given by

AF: Néel antiferromagnetic phase

$$x_0 = y_0 = \pi, \quad e_0^{\rm AF} = -1 + j_2 + j_3. \tag{7.7.23}$$

$\mathbf{AF_1}$: antiferromagnetic collinear order coincident with (7.7.10)

$$x_0 = 0, y_0 = \pi, \quad e_0^{\rm AF_1} = -j_2 + j_3. \tag{7.7.24}$$

$\mathbf{H_1}$: non-collinear order in which the spins are antiparallel along the $(1, 0)$ direction and make an angle $\pm y_0$ along the $(0, 1)$ direction

$$x_0 = \pi, \quad y_0 = \arccos\left(-\frac{1-2j_2}{4j_3}\right), \quad e_0^{\rm H_1} = -\frac{1}{2} - \frac{(1-2j_2)^2}{16j_3}. \tag{7.7.25}$$

$\mathbf{H_2}$: non-collinear order similar to Eq. (7.7.12)

$$x_0 = \pm y_0 = \arccos\left[-\frac{1}{2(j_2+2j_3)}\right], \quad e_0^{\rm H_2} = -j_3 - \frac{1}{4(j_2+2j_3)}. \tag{7.7.26}$$

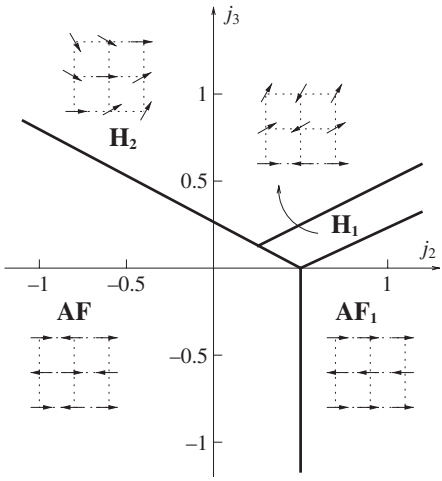

Fig. 7.12. Ground-state configurations of a SQ lattice with competing interactions $j_\alpha = \frac{J_\alpha}{J_1}$ and $J_1 < 0$.

The boundaries between the different regions shown in Fig. 7.12 are

$\mathbf{AF_1} - \mathbf{AF}$: $j_2 = \frac{1}{2}$,
$\mathbf{AF} - \mathbf{H_1}$ and $\mathbf{AF} - \mathbf{H_2}$: $j_3 = \frac{1}{4}(1 - 2j_2)$,
$\mathbf{AF_1} - \mathbf{H_1}$: $j_3 = -\frac{1}{4}(1 - 2j_2)$,
$\mathbf{H_1} - \mathbf{H_2}$: $j_3 = \frac{1}{2}j_2$.

The invariance of the energy under the exchange of x_0 with y_0 leads to the symmetric configurations obtained by the change of x_0 and y_0. Moreover, the disorder line $j_3 = \frac{1}{2}j_2$ remains also in the case $J_1 < 0$.

7.8. Frustration by Competing Interactions: Triangular Lattice

The ground-state energy of a TR lattice with $J_1 > 0$, NNN and TNN exchange interactions is given by

$$E_0^{\mathrm{TR}} = 6J_1S^2N\,e_0, \tag{7.8.1}$$

where

$$e_0 = -\gamma_{\boldsymbol{Q}}^{(1)} - j_2\gamma_{\boldsymbol{Q}}^{(2)} - j_3\gamma_{\boldsymbol{Q}}^{(3)} \tag{7.8.2}$$

with

$$\gamma_{\boldsymbol{Q}}^{(1)} = \frac{1}{3}(\cos 2y_0 + 2\cos x_0 \cos y_0), \tag{7.8.3}$$

$$\gamma_{\boldsymbol{Q}}^{(2)} = \frac{1}{3}(\cos 2x_0 + 2\cos x_0 \cos 3y_0), \tag{7.8.4}$$

$$\gamma_{\boldsymbol{Q}}^{(3)} = \frac{1}{3}(\cos 4y_0 + 2\cos 2x_0 \cos 2y_0) \tag{7.8.5}$$

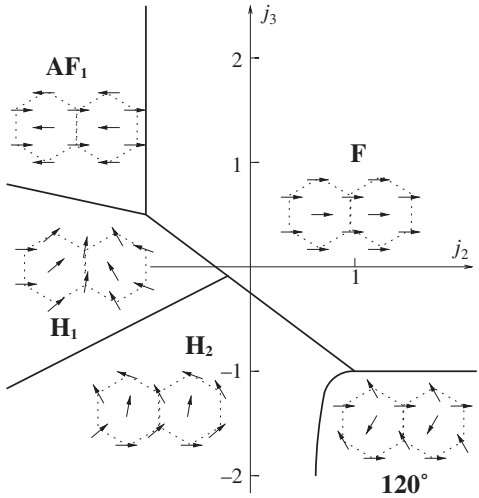

Fig. 7.13. Ground-state configurations of a TR lattice with competing interactions $j_\alpha = \frac{J_\alpha}{J_1}$ and $J_1 > 0$.

and

$$x_0 = \frac{\sqrt{3}}{2} a Q_x, \quad y_0 = \frac{1}{2} a Q_y, \quad j_\alpha = \frac{J_\alpha}{J_1}. \tag{7.8.6}$$

The minimum conditions are given by

$$\sin x_0[\cos y_0 + j_2(2\cos x_0 + \cos 3y_0) + 4j_3 \cos x_0 \cos 2y_0] = 0, \tag{7.8.7}$$

$$\sin y_0[2\cos y_0 + \cos x_0 + 3j_2 \cos x_0(4\cos^2 y_0 - 1) + 4j_3 \cos y_0(2\cos 2y_0 - \cos 2x_0)] = 0. \tag{7.8.8}$$

The minimum energy configurations in the $j_2 j_3$-plane are illustrated in Fig. 7.13. The $j_2 j_3$-plane is divided in five regions and the corresponding energies and helix wavevectors are given by

F: ferromagnetic phase

$$x_0 = y_0 = 0, \quad e_0^{\mathrm{F}} = -1 - j_2 - j_3. \tag{7.8.9}$$

$\mathbf{AF_1}$: antiferromagnetic collinear order with alternating lines of NNN parallel spins

$$x_0 = \pi, \quad y_0 = 0, \quad e_0^{\mathrm{AF}_1} = \frac{1}{3}(1 + j_2 - 3j_3). \tag{7.8.10}$$

$\mathbf{H_1}$: non-collinear order in which lines of NN spins are parallel while the spins of the adjacent NN line form an angle x_0:

$$y_0 = 0, \quad x_0 = \arccos\left[-\frac{1 + j_2}{2(j_2 + 2j_3)}\right], \quad e_0^{\mathrm{H}_1} = \frac{1}{2} j_2 + \frac{(1 - 2j_3)^2}{6(j_2 + 2j_3)}. \tag{7.8.11}$$

Two equivalent configurations are characterized by

$$x_0' = \arccos\left[\sqrt{\frac{-1+j_2+4j_3}{4(j_2+2j_3)}}\right], \quad y_0' = \pm x_0'. \tag{7.8.12}$$

One can verify that $2\cos^2 x_0' - 1 = \cos x_0$ so that $x_0' = x_0/2$ and the configurations obtained from Eq. (7.8.12) coincide with that shown in Fig. 7.13 given by Eq. (7.8.11) rotating the TR lattice by $\pm\frac{\pi}{3}$. In general, this magnetic order is *incommensurate* with the lattice periodicity.

$\mathbf{H_2}$: non-collinear order in which the spins are parallel along a NNN line and the spins in the adjacent NNN line form an angle y_0:

$$\begin{aligned} x_0 &= 0, \quad y_0 = \arccos\left[\frac{2j_3 - 3j_2 - \sqrt{(2j_3+3j_2)^2 - 8j_3}}{8j_3}\right], \\ e_0^{\mathrm{H}_2} &= -\frac{1}{3}(2\cos^2 y_0 + 2\cos y_0 - 1) - \frac{1}{3}j_2(8\cos^3 y_0 - 6\cos y_0 + 1) \\ &\quad - \frac{1}{3}j_3(8\cos^4 y_0 - 4\cos^2 y_0 - 1). \end{aligned} \tag{7.8.13}$$

Also in this case, two equivalent solutions exist

$$x_0' = \pm 3y_0', \quad y_0' = \arccos\left[\frac{10j_3 - 3j_2 - \sqrt{(3j_2+2j_3)^2 - 8j_3}}{16j_3}\right]^{\frac{1}{2}}. \tag{7.8.14}$$

One can verify that $y_0' = y_0/2$ and the two configurations given by Eq. (7.8.14) are obtained from that shown in Fig. 7.13 rotating the T lattice of an angle $\pm\frac{\pi}{3}$.

120°: a commensurate phase in which the spins of the magnetic cell form an angle $\frac{2\pi}{3}$ each other

$$x_0 = 0, \quad y_0 = \frac{2\pi}{3}, \quad e_0^{120^0} = \frac{1}{2}(1 - 2j_2 + j_3). \tag{7.8.15}$$

The boundaries between the different regions shown in Fig. 7.13 are lines of continuous (second order) phase transitions except the lines between regions **$\mathbf{AF_1} - \mathbf{F}$**, **$120^\circ - \mathbf{F}$** and **$120^\circ - \mathbf{H_2}$** where the transition is first order and **$\mathbf{H_1} - \mathbf{H_2}$** which is a disorder line. The equations of the separation lines between the different regions are

$\mathbf{AF_1} - \mathbf{F}$: $j_2 = -1$,
$\mathbf{F} - \mathbf{H_1}$ and **$\mathbf{F} - \mathbf{H_2}$**: $j_3 = -\frac{1}{4}(1 + 3j_2)$,
$\mathbf{AF_1} - \mathbf{H_1}$: $j_3 = \frac{1}{4}(1 - j_2)$,
$\mathbf{H_1} - \mathbf{H_2}$: $j_3 = \frac{1}{2}j_2$.
$120^\circ - \mathbf{F}$: $j_3 = -1$.
$120^\circ - \mathbf{H_2}$: $j_3 = \frac{j_2^2}{1-2j_2}$.

For $j_3 = \frac{1}{2}j_2$ Eqs. (7.8.7) and (7.8.8) are simultaneously satisfied assuming

$$1 + j_2(4\cos^2 y_0 + 4\cos x_0 \cos y_0 - 3) = 0 \tag{7.8.16}$$

so that a DH of equation

$$Q_y = 2\arccos\left[\frac{1}{2}\left(-\cos\frac{\sqrt{3}}{2}Q_x + \sqrt{3 + \cos^2\frac{\sqrt{3}}{2}Q_x - \frac{1}{j_2}}\right)\right] \tag{7.8.17}$$

occurs for any j_2 belonging to the line $j_3 = \frac{1}{2}j_2$. In Fig. 7.14, the DH lines are shown for $j_2 = -0.3, -0.5, -0.75, -1, -2, -10$ going from the inner to the outer curve. Notice that for $j_2 = -0.2$, the DH shrinks to the point $(0, 0)$. All the DH curves shown in Fig. 7.14 appear similar to circles. For instance, for $j_2 \to \infty$ the distance from the origin of the DH curve is in the range $2.09440 < |\boldsymbol{Q}| < 2.10557$.

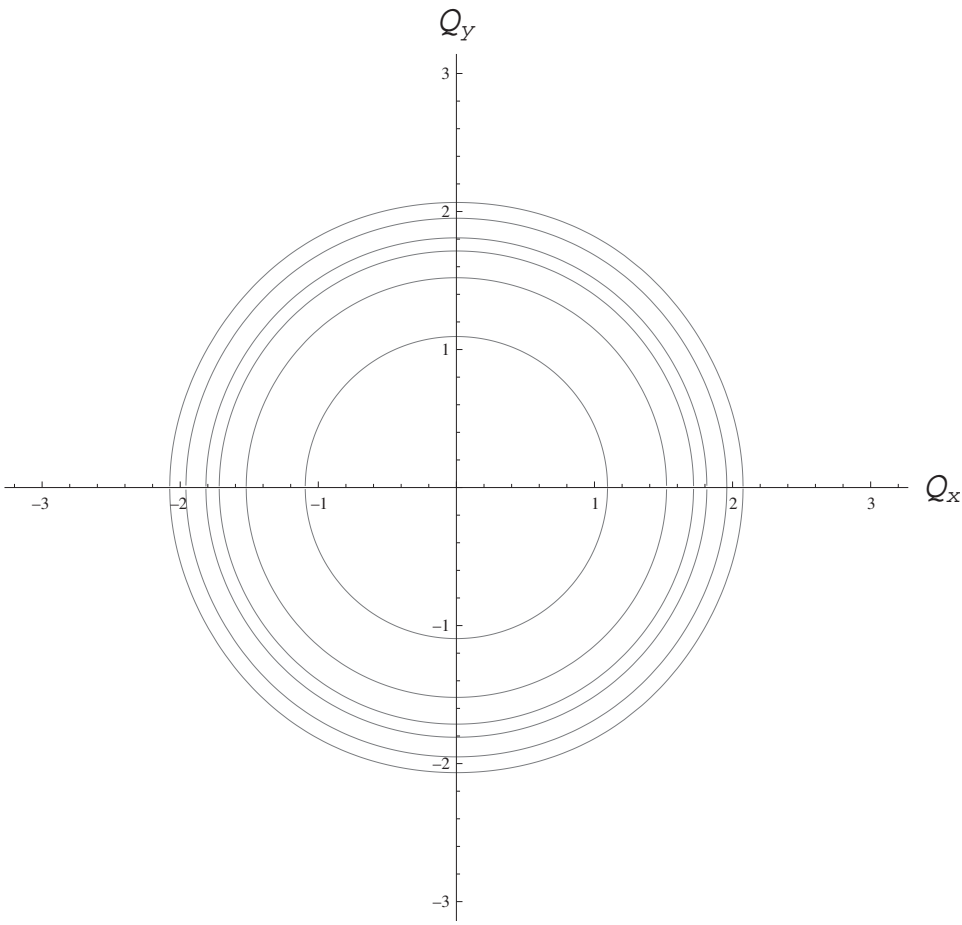

Fig. 7.14. Infinite degeneration line of the TR lattice in the reciprocal space for several j_2 ($j_3 = \frac{1}{2}j_2$). From the inner to the outer curve: $j_2 = -0.3$, -0.5, -0.75, -1, -2, -10, respectively.

Similarly, in the TR lattice as well as the SQ lattice, the quantum fluctuations destroy the DH. Indeed, the ground-state energy becomes

$$E_{\rm GS}^{\rm DH} = 6J_1S^2N\left\{\left[\frac{j_2}{2}+\frac{(1-j_2)^2}{12j_2}\right]\left(1+\frac{1}{S}\right)+\frac{\Delta}{S}\right\}, \tag{7.8.18}$$

where

$$\Delta = \frac{1}{(2\pi)^2}\int_{-\pi}^{\pi}dx\int_{-\pi}^{\pi}dy\sqrt{s(x,y)d_{\boldsymbol{Q}}(x,y)} \tag{7.8.19}$$

with

$$\begin{aligned} s(x,y) = &-\frac{1}{2}j_2-\frac{(1-j_2)^2}{12j_2}-\frac{1}{3}(\cos 2y+2\cos x\cos y)\\ &-\frac{1}{3}j_2(\cos 2x+2\cos x\cos 3y)-\frac{1}{6}j_2(\cos 4y+2\cos 2x\cos 2y), \end{aligned} \tag{7.8.20}$$

$$\begin{aligned} d_{\boldsymbol{Q}}(x,y) = &\frac{1}{3}[\cos 2y_0(1-\cos 2y)+2\cos x_0\cos y_0(1-\cos x\cos y)]\\ &+\frac{1}{3}j_2[\cos 2x_0(1-\cos 2x)+2\cos x_0\cos 3y_0(1-\cos x\cos 3y)]\\ &+\frac{1}{6}j_2[\cos 4y_0(1-\cos 4y)+2\cos 2x_0\cos 2y_0(1-\cos 2x\cos 2y)]\\ &-\frac{2}{3}\sin x_0\sin y_0\sin x\sin y-\frac{2}{3}j_2\sin x_0\sin 3y_0\sin x\sin 3y\\ &-\frac{1}{3}j_2\sin 2x_0\sin 2y_0\sin 2x\sin 2y \end{aligned} \tag{7.8.21}$$

and

$$y_0 = \arccos\left(-\frac{1}{2}\cos x_0+\frac{1}{2}\sqrt{3+\cos^2 x_0-\frac{1}{j_2}}\right). \tag{7.8.22}$$

For $|j_2| < 1.29$, the minima of the function Δ given by Eq. (7.8.19) are located along the directions $Q_x = 0$ and $Q_y = \pm\sqrt{3}Q_x$ corresponding to the six equivalent helices $\mathbf{H_1}$ and the maxima are located along the directions $Q_x = 0$ and $Q_y = \pm\frac{1}{\sqrt{3}}Q_x$ corresponding to the six equivalent helices $\mathbf{H_2}$. For $|j_2| > 2.4$, the maxima and minima are exchanged and the configuration corresponding to the helix $\mathbf{H_2}$ becomes stable. However, an unexpected event occurs for $1.29 < |j_2| < 2.4$ where the quantum fluctuations select neither the helix $\mathbf{H_1}$ nor the helix $\mathbf{H_2}$. New minima appear for $|j_2| = 1.29$ around the wavevectors of the $\mathbf{H_1}$ configuration that become maxima. By increasing $|j_2|$, the new minima move toward the neighbourhood of the wavevectors corresponding to the helix $\mathbf{H_2}$ and collapse into these wavevectors for $|j_2| = 2.4$. The above results imply that the existence region of the helix $\mathbf{H_1}$ widens for $|j_2| < 1.29$ and shrinks for $|j_2| > 2.4$ while a *new* phase appears for $1.29 < |j_2| < 2.4$ not expected from the classical result. This is a novelty that has never appeared in literature. The DH is also destroyed by adding the FNN exchange interaction $j_4 = \frac{2J_4}{J_1}$ to the classical ground-state energy of the TR lattice. The new phase

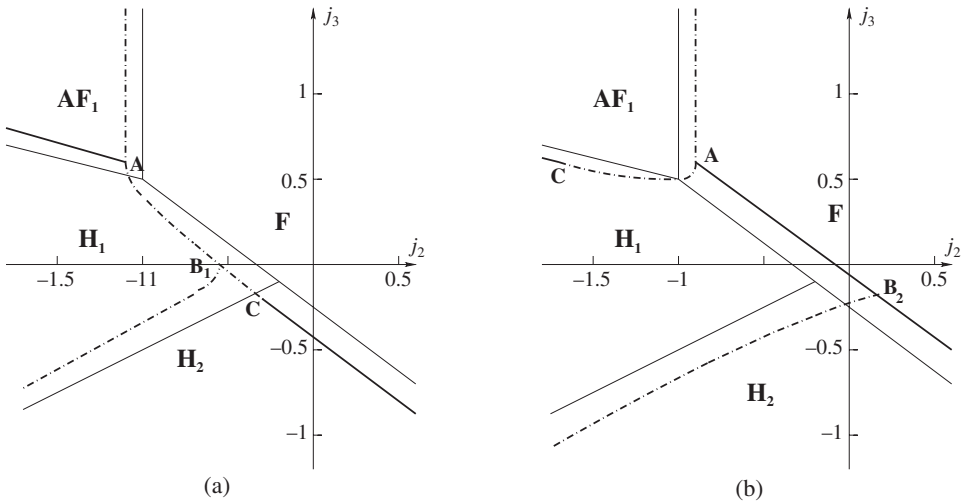

Fig. 7.15. Ground-state configurations of a TR lattice with competing interactions $j_\alpha = \frac{z_\alpha J_\alpha}{z_1 J_1}$ and $J_1 > 0$: thick lines (a) $j_4 = 0.1$; (b) $j_4 = -0.1$; thin lines $j_4 = 0$. The dashed-dotted lines mean first-order transition lines.

diagrams are shown in Fig. 7.15 (a) for $j_4 = 0.1$ and (b) for $j_4 = -0.1$, respectively. As one can see, the new phase diagrams are very rich. The dashed-dotted lines indicate first-order phase transitions while continuous lines mean second-order phase transitions. The thin lines refer to the case $j_4 = 0$ as shown in Fig. 7.13. As for the SQ lattice, a first-order transition line between the phases $\mathbf{H_1}$ and $\mathbf{H_2}$ replaces the DH (disorder) line. A variety of multicritical points appears in Fig. 7.15. The points A are the meeting of two first-order and one second-order transition lines. The point B_1 is the meeting of three first-order transition lines while the point B_2 is the meeting of two second-order and one first-order transition line. The points C are points in which a first-order transition changes to a second-order transition. Even though from Fig. 7.15(a) is not evident, the tangent of the curves meeting at the triple point $B_1(-0.5132, -0.0355)$ is the same.

The phase diagram at $T = 0$ of the H lattice with competing interactions in the basal (xy) plane is the same as that shown in Figs. 7.13 and 7.15. Indeed, the ground-state energy of the H lattice may be obtained from the TR energy (7.8.2) adding the out-of-plane interaction $j'\gamma'_{\boldsymbol{Q}}$ with $j' = J'/J_1$ and $\gamma'_{\boldsymbol{Q}} = \cos z_0$ ($z_0 = cQ_z$). The stacking of planes along the $(0, 0, 1)$ direction is ordered ferromagnetically ($z_0 = 0$) or antiferromagnetically ($z_0 = \pi$) according to $j' > 0$ or $j' < 0$, respectively. For the H lattice, the presence of the disorder line $j_3 = \frac{1}{2} j_2$ implies the absence of LRO at any finite temperature.

For $J_1 < 0$, the classical ground-state energy of the TR lattice becomes

$$E_0^{\mathrm{TR}} = 6|J_1|S^2 N e_0, \tag{7.8.23}$$

where

$$e_0 = \gamma_{\boldsymbol{Q}}^{(1)} + j_2 \gamma_{\boldsymbol{Q}}^{(2)} + j_3 \gamma_{\boldsymbol{Q}}^{(3)} \tag{7.8.24}$$

with $\gamma_{\boldsymbol{Q}}^{(\alpha)}$ given by Eqs. (7.8.3)–(7.8.5). The phase diagram at $T = 0$ is shown in Figs. 7.16–7.17. Fig. 7.17 is a magnification of the region delimited by the rectangle shown in Fig. 7.16. The $j_2 j_3$-plane is divided in six regions and the corresponding energies and helix wavevectors are given by:

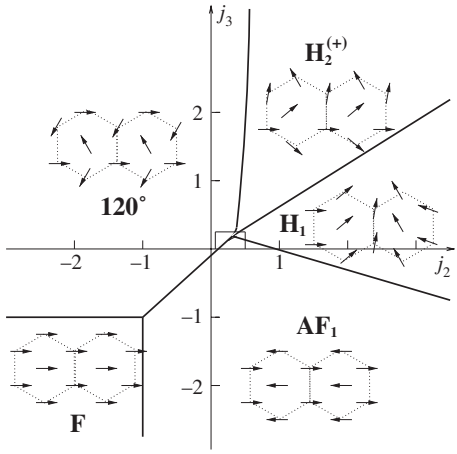

Fig. 7.16. Ground-state configurations of a TR lattice with competing interactions $j_\alpha = \frac{J_\alpha}{J_1}$ and $J_1 < 0$. The configurations inside the small rectangle with $\frac{1}{10} < j_2 < \frac{1}{2}$ and $0 < j_3 < \frac{1}{4}$ are shown in detail in Fig. 7.17.

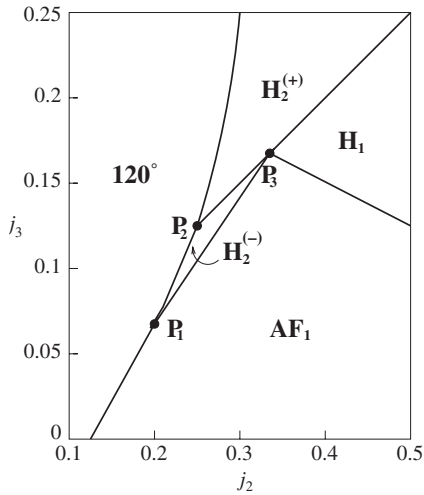

Fig. 7.17. Ground-state configurations of a TR lattice with competing interactions $j_\alpha = \frac{J_\alpha}{J_1}$ and $J_1 < 0$ for $\frac{1}{10} < j_2 < \frac{1}{2}$ and $0 < j_3 < \frac{1}{4}$.

F: ferromagnetic phase

$$x_0 = y_0 = 0, \quad e_0^{\mathrm{F}} = 1 + j_2 + j_3. \tag{7.8.25}$$

$\mathbf{AF_1}$: antiferromagnetic collinear order with alternating lines of NNN parallel spins

$$x_0 = \pi, \quad y_0 = 0, \quad e_0^{\mathrm{AF_1}} = -\frac{1}{3}(1 + j_2 - 3j_3). \tag{7.8.26}$$

In this configuration, four of the six NN spins of a given spin are antiparallel and two are parallel.

$\mathbf{H_1}$: non-collinear order in which lines of NN spins are parallel while the spins of the adjacent NN line form an angle x_0:

$$y_0 = 0, \quad x_0 = \arccos\left[-\frac{1 + j_2}{2(j_2 + 2j_3)}\right], \quad e_0^{\mathrm{H_1}} = -\frac{1}{2}j_2 - \frac{(1 - 2j_3)^2}{6(j_2 + 2j_3)}. \tag{7.8.27}$$

$\mathbf{H_2^{(\pm)}}$: non-collinear order in which the spins are parallel along a NNN line and the spins in the adjacent NNN line form an angle $y_0^{(\pm)}$:

$$x_0 = 0, \quad y_0^{(\pm)} = \arccos\left[\frac{2j_3 - 3j_2 \pm \sqrt{(2j_3 + 3j_2)^2 - 8j_3}}{8j_3}\right],$$

$$e_0^{\mathrm{H_2^{(\pm)}}} = \frac{1}{3}(2\cos^2 y_0^{(\pm)} + 2\cos y_0^{(\pm)} - 1) + \frac{1}{3}j_2(8\cos^3 y_0^{(\pm)} - 6\cos y_0^{(\pm)} + 1)$$
$$+\frac{1}{3}j_3(8\cos^4 y_0^{(\pm)} - 4\cos^2 y_0^{(\pm)} - 1). \tag{7.8.28}$$

$\mathbf{120^\circ}$: commensurate phase with

$$x_0 = 0, \quad y_0 = \frac{2\pi}{3}, \quad l_0^{120^\circ} = -\frac{1}{2}(1 - 2j_2 + j_3). \tag{7.8.29}$$

The boundaries between the different regions shown in Figs. 7.16 and 7.17 are first-order transition lines except the boundaries between the phases $\mathbf{AF_1} - \mathbf{H_1}$ and $\mathbf{AF_1} - \mathbf{H_2^{(-)}}$ where the transition is second order. The line between the phases $\mathbf{H_1} - \mathbf{H_2^{(+)}}$ and $\mathbf{H_2^{(-)}} - \mathbf{H_2^{(+)}}$ is a disorder line. The equations of the separation lines between the different regions are

$\mathbf{AF_1} - \mathbf{F}$: $j_2 = -1$,
$\mathbf{AF_1} - \mathbf{120^\circ}$: $j_3 = \frac{-1+8j_2}{9}$,
$\mathbf{AF_1} - \mathbf{H_2^{(-)}}$: $j_3 = \frac{-1+9j_2}{12}$,
$\mathbf{AF_1} - \mathbf{H_1}$: $j_3 = \frac{1-j_2}{4}$,
$\mathbf{H_2^{(+)}} - \mathbf{H_1}$ and $\mathbf{H_2^{(+)}} - \mathbf{H_2^{(-)}}$: $j_3 = \frac{1}{2}j_2$,
$\mathbf{120^\circ} - \mathbf{F}$: $j_3 = -1$.

The boundary line between the $\mathbf{120^\circ}$ and the $\mathbf{H_2^{(\pm)}}$ phases has to be evaluated numerically. The point $\mathrm{P_1}(\frac{1}{5}, \frac{1}{15})$ is a triple point where two first-order transition lines and one second-order transition line meet. The points $\mathrm{P_2}(\frac{1}{4}, \frac{1}{8})$ and $\mathrm{P_3}(\frac{1}{3}, \frac{1}{6})$ lie on the disorder line.

Concluding this section, it is worthwhile noticing that many magnetic compounds are made up of a staking of triangular planes. For instance, the members of the ABX_3 and BX_2 families where A is an alkali metal, B a transition metal and X a halogen[68] show a magnetic behaviour satisfactorily described by the triangular model discussed in this section.

7.9. Frustration by Competing Interaction: Honeycomb Lattice

In this section, we will study the classical ground state of a HON lattice. The novelty with respect to the SQ and TR lattices is that the HON lattice is not a Bravais lattice, that is, the primitive cell contains two non-equivalent lattice points so that the Hamiltonian (7.1.1) becomes

$$\mathcal{H} = -J_1 \sum_{i,\boldsymbol{\delta}_1} \left(\boldsymbol{S}_i^{(a)} \cdot \boldsymbol{S}_{i+\boldsymbol{\delta}_1}^{(b)} + \boldsymbol{S}_i^{(b)} \cdot \boldsymbol{S}_{i-\boldsymbol{\delta}_1}^{(a)} \right) - J_2 \sum_{i,\boldsymbol{\delta}_2} \left(\boldsymbol{S}_i^{(a)} \cdot \boldsymbol{S}_{i+\boldsymbol{\delta}_2}^{(a)} + \boldsymbol{S}_i^{(b)} \cdot \boldsymbol{S}_{i+\boldsymbol{\delta}_2}^{(b)} \right) - J_3 \sum_{i,\boldsymbol{\delta}_3} \left(\boldsymbol{S}_i^{(a)} \cdot \boldsymbol{S}_{i+\boldsymbol{\delta}_3}^{(b)} + \boldsymbol{S}_i^{(b)} \cdot \boldsymbol{S}_{i-\boldsymbol{\delta}_3}^{(a)} \right), \tag{7.9.1}$$

where a and b label the two non-equivalent atoms in the unit cell and i labels the lattice sites of *one* sublattice; $\boldsymbol{\delta}_1 = (\pm\frac{\sqrt{3}}{2}a, \frac{1}{2}a)$, $(0, -a)$; $\boldsymbol{\delta}_2 = (\pm\frac{\sqrt{3}}{2}a, \pm\frac{3}{2}a)$, $(\pm\sqrt{3}a, 0)$; $\boldsymbol{\delta}_3 = (\pm\sqrt{3}a, -a)$, $(0, 2a)$ are the lattice vectors joining the spin i with its three NN, six NNN and three TNN, respectively. With respect to the treatment of Section 7.1, we introduce an additional degree of freedom:[69] we consider the possibility that the non-equivalent spins in the unit cell make an angle α. The rotation matrix between cartesian and local axis is assumed to be of the form (7.1.2) with $\phi_i^{(a)} = \boldsymbol{Q} \cdot \boldsymbol{r}_i + \phi$ for the a-atoms and $\phi_i^{(b)} = \boldsymbol{Q} \cdot \boldsymbol{r}_i + \phi + \alpha$ for the b-atoms. Performing the following transformation to Bose operators

$$\begin{cases} S_i^{(a)\xi} = \dfrac{\sqrt{2S}}{2}\left(a_i + a_i^+\right), \\ S_i^{(a)\eta} = \dfrac{\sqrt{2S}}{2i}\left(a_i - a_i^+\right), \\ S_i^{(a)\zeta} = S - a_i^+ a_i, \end{cases} \qquad \begin{cases} S_i^{(b)\xi} = \dfrac{\sqrt{2S}}{2}\left(b_i + b_i^+\right), \\ S_i^{(b)\eta} = \dfrac{\sqrt{2S}}{2i}\left(b_i - b_i^+\right), \\ S_i^{(b)\zeta} = S - b_i^+ b_i, \end{cases} \tag{7.9.2}$$

we obtain the bilinear Hamiltonian

$$\mathcal{H}_2 = E_0 + \sum_{\boldsymbol{k}} A_{\boldsymbol{k}}(a_{\boldsymbol{k}}^+ a_{\boldsymbol{k}} + b_{\boldsymbol{k}}^+ b_{\boldsymbol{k}}) + \frac{1}{2}\sum_{\boldsymbol{k}} B_{\boldsymbol{k}}(a_{\boldsymbol{k}} a_{-\boldsymbol{k}} + a_{\boldsymbol{k}}^+ a_{-\boldsymbol{k}}^+ + b_{\boldsymbol{k}} b_{-\boldsymbol{k}} + b_{\boldsymbol{k}}^+ b_{-\boldsymbol{k}}^+) + \sum_{\boldsymbol{k}}(C_{\boldsymbol{k}}^* a_{\boldsymbol{k}} b_{-\boldsymbol{k}} + C_{\boldsymbol{k}} a_{\boldsymbol{k}}^+ b_{-\boldsymbol{k}}^+) + \sum_{\boldsymbol{k}}(D_{\boldsymbol{k}}^* a_{\boldsymbol{k}} b_{\boldsymbol{k}}^+ + D_{\boldsymbol{k}} a_{\boldsymbol{k}}^+ b_{\boldsymbol{k}}), \tag{7.9.3}$$

where

$$E_0 = -6J_1 S^2 N \left\{ \sin^2\theta \, \frac{1}{3}\sum_{\boldsymbol{\delta}_1} \cos(\boldsymbol{Q} \cdot \boldsymbol{\delta}_1 + \alpha) + \cos^2\theta + j_2 \left(\sin^2\theta \, \frac{1}{6}\sum_{\boldsymbol{\delta}_2} \cos \boldsymbol{Q} \cdot \boldsymbol{\delta}_2 + \cos^2\theta \right) \right.$$

$$+j_3\left[\sin^2\theta\ \frac{1}{3}\sum_{\boldsymbol{\delta}_3}\cos(\boldsymbol{Q}\cdot\boldsymbol{\delta}_3+\alpha)+\cos^2\theta\right]\Bigg\}, \tag{7.9.4}$$

$$A_{\boldsymbol{k}} = 6J_1S\Bigg\{\sin^2\theta\ \frac{1}{3}\sum_{\boldsymbol{\delta}_1}\cos(\boldsymbol{Q}\cdot\boldsymbol{\delta}_1+\alpha)+\cos^2\theta$$
$$+j_2\left(\sin^2\theta\ \frac{1}{6}\sum_{\boldsymbol{\delta}_2}\cos\boldsymbol{Q}\cdot\boldsymbol{\delta}_2+\cos^2\theta\right)$$
$$+j_3\left[\sin^2\theta\frac{1}{3}\sum_{\boldsymbol{\delta}_3}\cos(\boldsymbol{Q}\cdot\boldsymbol{\delta}_3+\alpha)+\cos^2\theta\right]-\frac{1}{12}j_2\left[\sin^2\theta\sum_{\boldsymbol{\delta}_2}\cos\boldsymbol{k}\cdot\boldsymbol{\delta}_2\right.$$
$$\left.+\frac{1}{2}(1+\cos\theta)^2\sum_{\boldsymbol{\delta}_2}\cos(\boldsymbol{k}+\boldsymbol{Q})\cdot\boldsymbol{\delta}_2+\frac{1}{2}(1-\cos\theta)^2\sum_{\boldsymbol{\delta}_2}\cos(\boldsymbol{k}-\boldsymbol{Q})\cdot\boldsymbol{\delta}_2\right]\Bigg\}, \tag{7.9.5}$$

$$B_{\boldsymbol{k}} = -\frac{1}{2}J_1S\ j_2\sin^2\theta\sum_{\boldsymbol{\delta}_2}\cos\boldsymbol{k}\cdot\boldsymbol{\delta}_2(1-\cos\boldsymbol{Q}\cdot\boldsymbol{\delta}_2), \tag{7.9.6}$$

$$C_{\boldsymbol{k}} = -J_1S\sin^2\theta\Bigg\{\sum_{\boldsymbol{\delta}_1}e^{i\boldsymbol{k}\cdot\boldsymbol{\delta}_1}[1-\cos(\boldsymbol{Q}\cdot\boldsymbol{\delta}_1+\alpha)]$$
$$+\ j_3\sum_{\boldsymbol{\delta}_3}e^{i\boldsymbol{k}\cdot\boldsymbol{\delta}_3}[1-\cos(\boldsymbol{Q}\cdot\boldsymbol{\delta}_3+\alpha)]\Bigg\} \tag{7.9.7}$$

and

$$D_{\boldsymbol{k}} = -J_1S\Bigg\{\sum_{\boldsymbol{\delta}_1}e^{i\boldsymbol{k}\cdot\boldsymbol{\delta}_1}[\sin^2\theta+(1+\cos^2\theta)\cos(\boldsymbol{Q}\cdot\boldsymbol{\delta}_1+\alpha)$$
$$+\ 2i\cos\theta\ \sin(\boldsymbol{Q}\cdot\boldsymbol{\delta}_1+\alpha)]$$
$$+j_3\sum_{\boldsymbol{\delta}_3}e^{i\boldsymbol{k}\cdot\boldsymbol{\delta}_3}[\sin^2\theta+(1+\cos^2\theta)\cos(\boldsymbol{Q}\cdot\boldsymbol{\delta}_3+\alpha)$$
$$+\ 2i\cos\theta\ \sin(\boldsymbol{Q}\cdot\boldsymbol{\delta}_3+\alpha)]\}, \tag{7.9.8}$$

where $j_2 = 2\frac{J_2}{J_1}$ and $j_3 = \frac{J_3}{J_1}$. The minimization of the classical ground-state energy E_0 given by Eq. (7.9.4) with respect to θ, α and $\boldsymbol{Q}$ leads to the phase diagrams shown in Figs. 7.18 and 7.19 for $J_1 > 0$ and $J_1 < 0$, respectively.

Assuming $J_1 > 0$ and introducing the reduced variables

$$e_0 = \frac{E_0}{6J_1S^2N}, \quad x_0 = \frac{\sqrt{3}}{2}aQ_x, \quad y_0 = \frac{1}{2}aQ_y \tag{7.9.9}$$

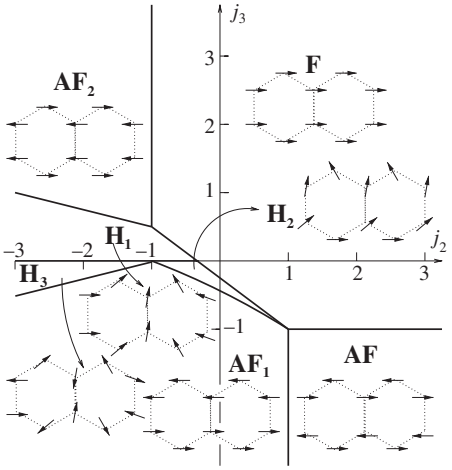

Fig. 7.18. Ground-state configurations of a HON lattice with competing interactions $j_\alpha = \frac{z_\alpha J_\alpha}{z_1 J_1}$ and $J_1 > 0$.

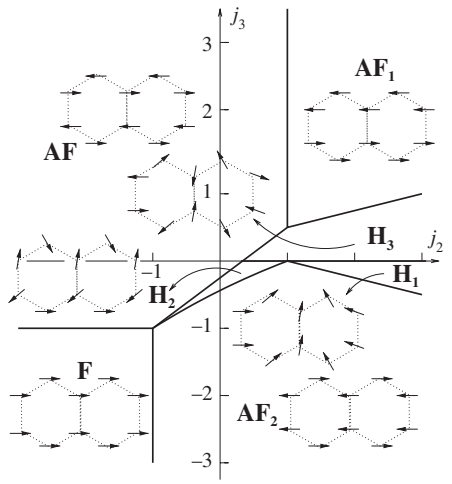

Fig. 7.19. Ground-state configurations of a HON lattice with competing interactions $j_\alpha = \frac{z_\alpha J_\alpha}{z_1 J_1}$ and $J_1 < 0$.

Equation (7.9.4) becomes

$$\begin{aligned} e_0 = -\frac{1}{3}\sin^2\theta\{&\cos(2y_0-\alpha)+2\cos x_0\cos(y_0+\alpha)\\ &+j_2(\cos 2x_0+2\cos x_0\cos 3y_0)\\ &+j_3[\cos(4y_0+\alpha)+2\cos 2x_0\cos(2y_0-\alpha)]\}\\ &-(1+j_2+j_3)\cos^2\theta. \end{aligned} \tag{7.9.10}$$

Imposing that the first partial derivatives of e_0 with respect to θ, x_0, y_0 and α vanish,

one obtains the following equations

$$\sin\theta\cos\theta\{1+j_2+j_3-\frac{1}{3}\left[\cos(2y_0-\alpha)+2\cos x_0\cos(y_0+\alpha)\right]$$
$$-\frac{1}{3}j_2(\cos 2x_0+2\cos x_0\cos 3y_0)-\frac{1}{3}j_3[\cos(4y_0+\alpha)$$
$$+2\cos 2x_0\cos(2y_0-\alpha)]\}=0, \tag{7.9.11}$$
$$\sin^2\theta\sin x_0[\cos(y_0+\alpha)+j_2(2\cos x_0+\cos 3y_0)$$
$$+4j_3\cos x_0\cos(2y_0-\alpha)]=0, \tag{7.9.12}$$
$$\sin^2\theta\{\sin(2y_0-\alpha)+\cos x_0\sin(y_0+\alpha)+3j_2\cos x_0\sin 3y_0$$
$$+2j_3[\sin(4y_0+\alpha)+\cos 2x_0\sin(2y_0-\alpha)]\}=0, \tag{7.9.13}$$
$$\sin^2\theta\{\sin(2y_0-\alpha)-2\cos x_0\sin(y_0+\alpha)$$
$$+j_3[2\cos 2x_0\sin(2y_0-\alpha)-\sin(4y_0+\alpha)]\}=0. \tag{7.9.14}$$

Equation (7.9.11) gives $\theta=\frac{\pi}{2}$ and the minimum energy configurations obtained from Eqs. (7.9.12)–(7.9.14) are shown in Fig. 7.18. The j_2j_3-plane is divided into seven regions: the spin configurations and reduced ground-state energy are

F: ferromagnetic phase

$$x_0=y_0=\alpha=0,\quad e_0^{\mathrm{F}}=-(1+j_2+j_3). \tag{7.9.15}$$

AF: antiferromagnetic collinear phase in which all three NN spins of a given spin are antiparallel (Néel antiferromagnet)

$$x_0=y_0=0,\quad \alpha=\pi,\quad e_0^{\mathrm{AF}}=1-j_2+j_3. \tag{7.9.16}$$

$\mathbf{AF_1}$: antiferromagnetic collinear phase in which one out of the three NN spins of a given spin is antiparallel and two are parallel

$$x_0=0,\quad y_0=\frac{\pi}{3},\quad \alpha=-\frac{\pi}{3},\quad e_0^{\mathrm{AF_1}}=-\frac{1}{3}(1-j_2-3j_3). \tag{7.9.17}$$

$\mathbf{AF_2}$: antiferromagnetic collinear phase in which two of the three NN spins of a given spin are antiparallel and one is parallel

$$x_0=\pi,\quad y_0=\alpha=0,\quad e_0^{\mathrm{AF_2}}=\frac{1}{3}(1+j_2-3j_3). \tag{7.9.18}$$

$\mathbf{H_1}$: helical phase with zero angle between the two non-equivalent spins

$$x_0=\arccos\left[-\frac{1+j_2}{2(j_2+2j_3)}\right],\quad y_0=\alpha=0,$$
$$e_0^{\mathrm{H_1}}=\frac{1}{2}j_2+\frac{(1-2j_3)^2}{6(j_2+2j_3)}. \tag{7.9.19}$$

$\mathbf{H_2}$: helical phase with an angle between the two non-equivalent spins different from 0 and π

$$x_0 = 0,$$

$$y_0 = \frac{1}{3}\arccos\left\{-\frac{1}{2j_3(1+2j_3)}\left[1+3j_3+j_2(1+j_3)\sqrt{\frac{(1+j_3)(1-2j_3)}{j_2^2-j_3(1+2j_3)}}\right]\right\},$$

$$\alpha = -y_0 + \arctan\frac{(1+j_3)\sin 3y_0}{2+(1+3j_3)\cos 3y_0},$$

$$e_0^{\mathrm{H}_2} = -\frac{1}{3}\{\cos(2y_0-\alpha)+2\cos(y_0+\alpha)+j_2(1+2\cos 3y_0)$$
$$+j_3[\cos(4y_0+\alpha)+2\cos(2y_0-\alpha)]\}. \tag{7.9.20}$$

$\mathbf{H_3}$: helical phase with an angle π between the two non-equivalent spins

$$x_0 = \arccos\left[\frac{1-j_2}{2(j_2-2j_3)}\right], y_0 = 0, \quad \alpha = \pi,$$

$$e_0^{\mathrm{H}_3} = \frac{1}{2}j_2 + \frac{(1-2j_3)^2}{6(j_2-2j_3)}. \tag{7.9.21}$$

The boundaries between the different regions shown in Fig. 7.18 are first-order transition lines except the boundaries between the phases $\mathbf{F}-\mathbf{H_1}$, $\mathbf{F}-\mathbf{H_2}$, $\mathbf{AF_1}-\mathbf{H_2}$, $\mathbf{AF_1}-\mathbf{H_3}$ and $\mathbf{AF_2}-\mathbf{H_1}$ where the transition is second order. The transition line between the $\mathbf{H_1}$ and $\mathbf{H_2}$, $\mathbf{H_3}$ phases is a disorder line. Indeed, for $j_3 = 0$ and $j_2 < -\frac{1}{3}$ the ground state is infinitely degenerate: the equation of the DH line is

$$Q_y = \frac{2}{3a}\arccos\left[\frac{1-j_2^2\left(1+4\cos^2\frac{\sqrt{3}}{2}aQ_x\right)}{4j_2^2\cos\frac{\sqrt{3}}{2}aQ_x}\right]. \tag{7.9.22}$$

The DH line reduces to the point $(0,0)$ at $j_2 = -\frac{1}{3}$, it forms closed curves around the origin for $-1 < j_2 < -\frac{1}{3}$. These closed curves become circles for $j_2 \to -\frac{1}{3}$ and a rhombus for $j_2 \to -1$. For $j_2 < -1$, the closed curves are pseudo-triangle centred around the point $(0, \frac{4\pi}{3\sqrt{3}a})$ and the symmetric points obtained rotating by 60, 120, 180, 240, 300 degrees. The equations of the separation lines between the different regions are

$\mathbf{F}-\mathbf{AF}$: $j_3 = -1$,
$\mathbf{F}-\mathbf{AF_2}$: $j_2 = -1$,
$\mathbf{F}-\mathbf{H_1}$ and $\mathbf{F}-\mathbf{H_2}$: $j_3 = -\frac{1+3j_2}{4}$,
$\mathbf{AF}-\mathbf{AF_1}$: $j_2 = 1$,
$\mathbf{AF_1}-\mathbf{H_2}$: $j_3 = \frac{1}{8}(1-3j_2-\sqrt{9j_2^2+10j_2+17})$,
$\mathbf{AF_1}-\mathbf{H_3}$: $j_3 = \frac{1+j_2}{4}$,
$\mathbf{AF_2}-\mathbf{H_1}$: $j_3 = \frac{1-j_2}{4}$,
$\mathbf{H_1}-\mathbf{H_2}$ and $\mathbf{H_1}-\mathbf{H_3}$: $j_3 = 0$.

For $J_1 < 0$, the phase diagram at $T = 0$ is shown in Fig. 7.19. In the present case, the reduced quantities are the same as those given in Eq. (7.9.9) except that J_1 has to be replaced by $|J_1|$. The $j_2 j_3$-plane is divided into seven regions: the spin configurations and reduced ground-state energies are

F: ferromagnetic phase

$$x_0 = y_0 = \alpha = 0, \quad e_0^{\mathrm{F}} = 1 + j_2 + j_3. \tag{7.9.23}$$

AF: Néel antiferromagnetic collinear phase

$$x_0 = y_0 = 0, \quad \alpha = \pi, \quad e_0^{\mathrm{AF}} = -1 + j_2 - j_3. \tag{7.9.24}$$

$\mathbf{AF_1}$: antiferromagnetic collinear phase in which one out of the three NN spins of a given spin is antiparallel and two are parallel

$$x_0 = 0, \quad y_0 = \frac{\pi}{3}, \quad \alpha = -\frac{\pi}{3}, \quad e_0^{\mathrm{AF_1}} = \frac{1}{3}(1 - j_2 - 3j_3). \tag{7.9.25}$$

$\mathbf{AF_2}$: antiferromagnetic collinear phase in which two of the three NN spins of a given spin are antiparallel and one is parallel

$$x_0 = \pi, \quad y_0 = \alpha = 0, \quad e_0^{\mathrm{AF_2}} = -\frac{1}{3}(1 + j_2 - 3j_3). \tag{7.9.26}$$

$\mathbf{H_1}$: helical phase with zero angle between the two non-equivalent spins

$$\begin{aligned} x_0 &= \arccos\left[-\frac{1 + j_2}{2(j_2 + 2j_3)}\right], \quad y_0 = \alpha = 0, \\ e_0^{\mathrm{H_1}} &= -\frac{1}{2} j_2 - \frac{(1 - 2j_3)^2}{6(j_2 + 2j_3)}. \end{aligned} \tag{7.9.27}$$

$\mathbf{H_2}$: helical phase with an angle $\alpha \neq 0, \pi$ between the two non-equivalent spins

$$\begin{aligned} x_0 &= 0, \\ y_0 &= \frac{1}{3} \arccos\left\{-\frac{1}{2j_3(1 + 2j_3)}\left[1 + 3j_3 + j_2(1 + j_3)\sqrt{\frac{(1 + j_3)(1 - 2j_3)}{j_2^2 - j_3(1 + 2j_3)}}\right]\right\}, \\ \alpha &= -y_0 + \arctan\frac{(1 + j_3)\sin 3y_0}{2 + (1 + 3j_3)\cos 3y_0}, \\ e_0^{\mathrm{H_2}} &= \frac{1}{3}\left\{\cos(2y_0 - \alpha) + 2\cos(y_0 + \alpha) + j_2(1 + 2\cos 3y_0)\right. \\ &\quad \left. + j_3\left[\cos(4y_0 + \alpha) + 2\cos(2y_0 - \alpha)\right]\right\}. \end{aligned} \tag{7.9.28}$$

$\mathbf{H_3}$: helical phase with an angle π between the two non-equivalent spins

$$\begin{aligned} x_0 &= \arccos\left[\frac{1 - j_2}{2(j_2 - 2j_3)}\right], \quad y_0 = 0, \quad \alpha = \pi, \\ e_0^{\mathrm{H_3}} &= -\frac{1}{2} j_2 - \frac{(1 - 2j_3)^2}{6(j_2 - 2j_3)}. \end{aligned} \tag{7.9.29}$$

The boundaries between the different regions shown in Fig. 7.19 are first-order transition lines except the boundaries between the phases $\mathbf{AF}-\mathbf{H_2}$, $\mathbf{AF}-\mathbf{H_3}$, $\mathbf{AF_1}-\mathbf{H_3}$, $\mathbf{AF_2}-\mathbf{H_1}$ and $\mathbf{AF_2}-\mathbf{H_2}$ where the transition is second order. The $\mathbf{H_3}-\mathbf{H_2}$ and $\mathbf{H_3}-\mathbf{H_1}$ boundary line ($j_3=0$) is a disorder line. The equations of the separation lines between the different regions are

$\mathbf{AF}-\mathbf{F}$: $j_3=-1$,
$\mathbf{AF}-\mathbf{H_2}$ and $\mathbf{AF}-\mathbf{H_3}$: $j_3=-\frac{1-3j_2}{4}$,
$\mathbf{AF}-\mathbf{AF_1}$: $j_2=1$,
$\mathbf{AF_1}-\mathbf{H_3}$: $j_3=\frac{1+j_2}{4}$,
$\mathbf{AF_2}-\mathbf{H_2}$: $j_3=\frac{1}{8}(1+3j_2-\sqrt{9j_2^2-10j_2+17})$,
$\mathbf{AF_2}-\mathbf{H_1}$: $j_3=\frac{1-j_2}{4}$,
$\mathbf{AF_2}-\mathbf{F}$: $j_2=-1$,
$\mathbf{H_3}-\mathbf{H_2}$ and $\mathbf{H_3}-\mathbf{H_1}$: $j_3=0$.

To obtain the spin wave spectrum of the HON lattice with competing interaction, we have to diagonalize the harmonic Hamiltonian (7.9.3). To do this, we use a procedure different from that used in Sec. 7.2. Instead of making use of the Bogoliubov transformation (7.2.2), we introduce the more general transformation

$$\alpha_{\boldsymbol{k}}^{(i)}=u_{\boldsymbol{k}}^{(i)}a_{\boldsymbol{k}}-l_{\boldsymbol{k}}^{(i)}a_{-\boldsymbol{k}}^{+}+v_{\boldsymbol{k}}^{(i)}b_{\boldsymbol{k}}-m_{\boldsymbol{k}}^{(i)}b_{-\boldsymbol{k}}^{+} \tag{7.9.30}$$

in order to transform the Hamiltonian (7.9.3) into the diagonal Hamiltonian

$$\mathcal{H}_2=E_0'+\sum_i\sum_{\boldsymbol{k}}\hbar\omega_{\boldsymbol{k}}^{(i)}\alpha_{\boldsymbol{k}}^{(i)+}\alpha_{\boldsymbol{k}}^{(i)} \tag{7.9.31}$$

The number of the new operators $\alpha_{\boldsymbol{k}}^{(i)}$ will be established by the determinant equation generated by the transformation (7.9.30) and by the requirement of stability, that is the frequences $\omega_{\boldsymbol{k}}^{(i)}$ appearing in Eq. (7.9.31) have to be positive. From Eqs. (7.9.30), one obtains directly the transformations for $\alpha_{-\boldsymbol{k}}^{+}$ assuming that $u_{-\boldsymbol{k}}^{(i)}=u_{\boldsymbol{k}}^{(i)*}$, $l_{-\boldsymbol{k}}^{(i)}=l_{\boldsymbol{k}}^{(i)*}$, $v_{-\boldsymbol{k}}^{(i)}=v_{\boldsymbol{k}}^{(i)*}$ and $m_{-\boldsymbol{k}}^{(i)}=m_{\boldsymbol{k}}^{(i)*}$. Moreover, the condition that the new operators $\alpha_{\boldsymbol{k}}^{(i)}$, as well as $a_{\boldsymbol{k}}$ and $b_{\boldsymbol{k}}$ are Bose operators, implies that

$$|u_{\boldsymbol{k}}^{(i)}|^2-|l_{\boldsymbol{k}}^{(i)}|^2+|v_{\boldsymbol{k}}^{(i)}|^2-|m_{\boldsymbol{k}}^{(i)}|^2=1. \tag{7.9.32}$$

The commutators of the operators $a_{\boldsymbol{k}}$, $a_{-\boldsymbol{k}}^{+}$, $b_{\boldsymbol{k}}$ and $b_{-\boldsymbol{k}}^{+}$ occurring in Eqs. (7.9.30) with the Hamiltonian (7.9.3) give

$$[a_{\boldsymbol{k}},\mathcal{H}_2]=A_{\boldsymbol{k}}a_{\boldsymbol{k}}+B_{\boldsymbol{k}}a_{-\boldsymbol{k}}^{+}+C_{\boldsymbol{k}}b_{-\boldsymbol{k}}^{+}+D_{\boldsymbol{k}}b_{\boldsymbol{k}}, \tag{7.9.33}$$

$$[a_{-\boldsymbol{k}}^{+},\mathcal{H}_2]=-A_{\boldsymbol{k}}a_{-\boldsymbol{k}}^{+}-B_{\boldsymbol{k}}a_{\boldsymbol{k}}-C_{\boldsymbol{k}}b_{\boldsymbol{k}}-D_{\boldsymbol{k}}b_{-\boldsymbol{k}}^{+}, \tag{7.9.34}$$

$$[b_{\boldsymbol{k}},\mathcal{H}_2]=A_{\boldsymbol{k}}b_{\boldsymbol{k}}+B_{\boldsymbol{k}}b_{-\boldsymbol{k}}^{+}+C_{\boldsymbol{k}}^{*}a_{-\boldsymbol{k}}^{+}+D_{\boldsymbol{k}}^{*}a_{\boldsymbol{k}} \tag{7.9.35}$$

and

$$[b_{-\boldsymbol{k}}^{+},\mathcal{H}_2]=-A_{\boldsymbol{k}}b_{-\boldsymbol{k}}^{+}-B_{\boldsymbol{k}}b_{\boldsymbol{k}}-C_{\boldsymbol{k}}^{*}a_{\boldsymbol{k}}-D_{\boldsymbol{k}}^{*}a_{-\boldsymbol{k}}^{+}, \tag{7.9.36}$$

so that the commutator of the operator $\alpha_{\boldsymbol{k}}^{(i)}$ with the Hamiltonian (7.9.3) becomes

$$\begin{aligned}[\alpha_{\boldsymbol{k}}^{(i)}, \mathcal{H}_2] = &(A_{\boldsymbol{k}} u_{\boldsymbol{k}}^{(i)} + B_{\boldsymbol{k}} l_{\boldsymbol{k}}^{(i)} + D_{\boldsymbol{k}}^* v_{\boldsymbol{k}}^{(i)} + C_{\boldsymbol{k}}^* m_{\boldsymbol{k}}^{(i)}) a_{\boldsymbol{k}} \\ &+ (B_{\boldsymbol{k}} u_{\boldsymbol{k}}^{(i)} + A_{\boldsymbol{k}} l_{\boldsymbol{k}}^{(i)} + C_{\boldsymbol{k}}^* v_{\boldsymbol{k}}^{(i)} + D_{\boldsymbol{k}}^* m_{\boldsymbol{k}}^{(i)}) a_{-\boldsymbol{k}}^+ \\ &+ (D_{\boldsymbol{k}} u_{\boldsymbol{k}}^{(i)} + C_{\boldsymbol{k}} l_{\boldsymbol{k}}^{(i)} + A_{\boldsymbol{k}} v_{\boldsymbol{k}}^{(i)} + B_{\boldsymbol{k}} m_{\boldsymbol{k}}^{(i)}) b_{\boldsymbol{k}} \\ &+ (C_{\boldsymbol{k}} u_{\boldsymbol{k}}^{(i)} + D_{\boldsymbol{k}} l_{\boldsymbol{k}}^{(i)} + B_{\boldsymbol{k}} v_{\boldsymbol{k}}^{(i)} + A_{\boldsymbol{k}} m_{\boldsymbol{k}}^{(i)}) b_{-\boldsymbol{k}}^+. \end{aligned} \tag{7.9.37}$$

The coefficients of the transformation (7.9.30) that bring the Hamiltonian (7.9.3) into the diagonal Hamiltonian (7.9.31) are determined comparing the commutator of $\alpha_{\boldsymbol{k}}^{(i)}$ with the Hamiltonian (7.9.31), that is

$$[\alpha_{\boldsymbol{k}}^{(i)}, \mathcal{H}_2] = \hbar\omega_{\boldsymbol{k}}^{(i)} \alpha_{\boldsymbol{k}}^{(i)} = \hbar\omega_{\boldsymbol{k}}^{(i)} (u_{\boldsymbol{k}}^{(i)} a_{\boldsymbol{k}} - l_{\boldsymbol{k}}^{(i)} a_{-\boldsymbol{k}}^+ + v_{\boldsymbol{k}}^{(i)} b_{\boldsymbol{k}} - m_{\boldsymbol{k}}^{(i)} b_{-\boldsymbol{k}}^+) \tag{7.9.38}$$

with Eq. (7.9.37). By equating Eqs. (7.9.37) and (7.9.38) one obtains a linear homogeneous system in the coefficients that can be written in a matrix form as

$$\begin{pmatrix} A_{\boldsymbol{k}} - \hbar\omega_{\boldsymbol{k}}^{(i)} & B_{\boldsymbol{k}} & D_{\boldsymbol{k}}^* & C_{\boldsymbol{k}}^* \\ B_{\boldsymbol{k}} & A_{\boldsymbol{k}} + \hbar\omega_{\boldsymbol{k}}^{(i)} & C_{\boldsymbol{k}}^* & D_{\boldsymbol{k}}^* \\ D_{\boldsymbol{k}} & C_{\boldsymbol{k}} & A_{\boldsymbol{k}} - \hbar\omega_{\boldsymbol{k}}^{(i)} & B_{\boldsymbol{k}} \\ C_{\boldsymbol{k}} & D_{\boldsymbol{k}} & B_{\boldsymbol{k}} & A_{\boldsymbol{k}} + \hbar\omega_{\boldsymbol{k}}^{(i)} \end{pmatrix} \begin{pmatrix} u_{\boldsymbol{k}}^{(i)} \\ l_{\boldsymbol{k}}^{(i)} \\ v_{\boldsymbol{k}}^{(i)} \\ m_{\boldsymbol{k}}^{(i)} \end{pmatrix} = 0. \tag{7.9.39}$$

The non-trivial solutions of this matrix equation are obtained by imposing that the determinant of the square matrix appearing in Eq. (7.9.39) is zero. So doing one obtains a biquadratic equation in $\omega_{\boldsymbol{k}}^{(i)}$ the solutions of which are

$$\begin{aligned}[\hbar\omega_{\boldsymbol{k}}^{(i)}]^2 = &A_{\boldsymbol{k}}^2 - B_{\boldsymbol{k}}^2 - |C_{\boldsymbol{k}}|^2 + |D_{\boldsymbol{k}}|^2 \\ &\mp \sqrt{4|A_{\boldsymbol{k}} D_{\boldsymbol{k}} - B_{\boldsymbol{k}} C_{\boldsymbol{k}}|^2 + (C_{\boldsymbol{k}} D_{\boldsymbol{k}}^* - C_{\boldsymbol{k}}^* D_{\boldsymbol{k}})^2}. \end{aligned} \tag{7.9.40}$$

The square root of Eq. (7.9.38) leads to four frequencies for $\omega_{\boldsymbol{k}}^{(i)}$ two of which are positive. The two negative roots have to be rejected for stability reasons and the two positive roots give the spin wave spectra of the bilinear Hamiltonian (7.9.31), that is,

$$\begin{aligned}\hbar\omega_{\boldsymbol{k}}^{(\mp)} = \Big[&A_{\boldsymbol{k}}^2 - B_{\boldsymbol{k}}^2 - |C_{\boldsymbol{k}}|^2 + |D_{\boldsymbol{k}}|^2 \\ &\mp \sqrt{4|A_{\boldsymbol{k}} D_{\boldsymbol{k}} - B_{\boldsymbol{k}} C_{\boldsymbol{k}}|^2 + (C_{\boldsymbol{k}} D_{\boldsymbol{k}}^* - C_{\boldsymbol{k}}^* D_{\boldsymbol{k}})^2}\Big]^{\frac{1}{2}}. \end{aligned} \tag{7.9.41}$$

The coefficients of the transformation (7.9.30) are given by

$$\begin{aligned}l_{\boldsymbol{k}}^{(\mp)} = \frac{u_{\boldsymbol{k}}^{(\mp)}}{\Delta_{\boldsymbol{k}}^{(\mp)}} \Big[&A_{\boldsymbol{k}} (C_{\boldsymbol{k}}^* D_{\boldsymbol{k}} + C_{\boldsymbol{k}} D_{\boldsymbol{k}}^*) - 2B_{\boldsymbol{k}} |C_{\boldsymbol{k}}|^2 + (C_{\boldsymbol{k}}^* D_{\boldsymbol{k}} - C_{\boldsymbol{k}} D_{\boldsymbol{k}}^*) \hbar\omega_{\boldsymbol{k}}^{(\mp)} \\ &\mp B_{\boldsymbol{k}} \sqrt{4|A_{\boldsymbol{k}} D_{\boldsymbol{k}} - B_{\boldsymbol{k}} C_{\boldsymbol{k}}|^2 + (C_{\boldsymbol{k}} D_{\boldsymbol{k}}^* - C_{\boldsymbol{k}}^* D_{\boldsymbol{k}})^2}\Big], \end{aligned} \tag{7.9.42}$$

$$v_{\boldsymbol{k}}^{(\mp)} = \frac{u_{\boldsymbol{k}}^{(\mp)}|}{\Delta_{\boldsymbol{k}}^{(\mp)}} \Big[2A_{\boldsymbol{k}}B_{\boldsymbol{k}}C_{\boldsymbol{k}} - D_{\boldsymbol{k}}(2A_{\boldsymbol{k}}^2 - |C_{\boldsymbol{k}}|^2) - C_{\boldsymbol{k}}^2 D_{\boldsymbol{k}}^* - 2(A_{\boldsymbol{k}}D_{\boldsymbol{k}} - B_{\boldsymbol{k}}C_{\boldsymbol{k}})\hbar\omega_{\boldsymbol{k}}^{(\mp)}$$

$$\pm D_{\boldsymbol{k}}\sqrt{4|A_{\boldsymbol{k}}D_{\boldsymbol{k}} - B_{\boldsymbol{k}}C_{\boldsymbol{k}}|^2 + (C_{\boldsymbol{k}}D_{\boldsymbol{k}}^* - C_{\boldsymbol{k}}^* D_{\boldsymbol{k}})^2}\Big], \tag{7.9.43}$$

$$m_{\boldsymbol{k}}^{(\mp)} = \frac{u_{\boldsymbol{k}}^{(\mp)}}{\Delta_{\boldsymbol{k}}^{(\mp)}} \Big[2A_{\boldsymbol{k}}B_{\boldsymbol{k}}D_{\boldsymbol{k}} - C_{\boldsymbol{k}}(2B_{\boldsymbol{k}}^2 - |D_{\boldsymbol{k}}|^2) - C_{\boldsymbol{k}}^* D_{\boldsymbol{k}}^2$$

$$\mp C_{\boldsymbol{k}}\sqrt{4|A_{\boldsymbol{k}}D_{\boldsymbol{k}} - B_{\boldsymbol{k}}C_{\boldsymbol{k}}|^2 + (C_{\boldsymbol{k}}D_{\boldsymbol{k}}^* - C_{\boldsymbol{k}}^* D_{\boldsymbol{k}})^2}\Big] \tag{7.9.44}$$

with

$$\Delta_{\boldsymbol{k}}^{(\mp)} = -2A_{\boldsymbol{k}}|D_{\boldsymbol{k}}|^2 + B_{\boldsymbol{k}}(C_{\boldsymbol{k}}^* D_{\boldsymbol{k}} + C_{\boldsymbol{k}}D_{\boldsymbol{k}}^*)$$

$$\pm(A_{\boldsymbol{k}} + \hbar\omega_{\boldsymbol{k}}^{(\mp)})\sqrt{4|A_{\boldsymbol{k}}D_{\boldsymbol{k}} - B_{\boldsymbol{k}}C_{\boldsymbol{k}}|^2 + (C_{\boldsymbol{k}}D_{\boldsymbol{k}}^* - C_{\boldsymbol{k}}^* D_{\boldsymbol{k}})^2}. \tag{7.9.45}$$

The value of $|u_{\boldsymbol{k}}^{(\mp)}|$ is determined by the condition (7.9.32). The "inverse" transformations of Eqs. (7.9.30) that is the transformation from a and b to $\alpha^{(i)}$ $(i = 1, 2)$ is given by

$$a_{\boldsymbol{k}} = u_{\boldsymbol{k}}^{(-)*}\alpha_{\boldsymbol{k}}^{(1)} + l_{\boldsymbol{k}}^{(-)*}\alpha_{-\boldsymbol{k}}^{(1)+} + u_{\boldsymbol{k}}^{(+)*}\alpha_{\boldsymbol{k}}^{(2)} + l_{\boldsymbol{k}}^{(+)*}\alpha_{-\boldsymbol{k}}^{(2)+} \tag{7.9.46}$$

and

$$b_{\boldsymbol{k}} = v_{\boldsymbol{k}}^{(-)*}\alpha_{\boldsymbol{k}}^{(1)} + m_{\boldsymbol{k}}^{(-)*}\alpha_{-\boldsymbol{k}}^{(1)+} + v_{\boldsymbol{k}}^{(+)*}\alpha_{\boldsymbol{k}}^{(2)} + m_{\boldsymbol{k}}^{(+)*}\alpha_{-\boldsymbol{k}}^{(2)+}. \tag{7.9.47}$$

Using Eqs. (7.9.46) and (7.9.47) and (7.9.3), one can obtain the zero-point energy. From Eq. (7.9.31), one obtains

$$E_0^{'} = E_0 + \Delta E_0, \tag{7.9.48}$$

where

$$\Delta E_0 = -\sum_{\boldsymbol{k}} \hbar\omega_{\boldsymbol{k}}^{(-)}(|l_{\boldsymbol{k}}^{(-)}|^2 + |m_{\boldsymbol{k}}^{(-)}|^2) - \sum_{\boldsymbol{k}} \hbar\omega_{\boldsymbol{k}}^{(+)}(|l_{\boldsymbol{k}}^{(+)}|^2 + |m_{\boldsymbol{k}}^{(+)}|^2). \tag{7.9.49}$$

7.10. Neutron Scattering Cross-Section for a Helimagnet

In this section, we will evaluate the neutron cross-section for a system with non-collinear order. The starting point is the magnetic neutron cross-section given by Eq. (3.1.1) and (3.1.2). To simplify the calculations, we will restrict ourselves to the harmonic approximation so that we disregard damping and renormalization of the spin waves. The first step consists of writing the structure factor (3.1.2) in terms of the spin components along the local axis. To do this, we make use of the rotation

matrix (7.1.2) with $\theta = \frac{\pi}{2}$. In this way, the spins lie in the xy-plane. We begin evaluating the correlation function $\langle S_i^x S_j^x(t)\rangle$, that is,

$$\langle S_i^x S_j^x(t)\rangle = \sin \boldsymbol{Q}\cdot\boldsymbol{r}_i \sin \boldsymbol{Q}\cdot\boldsymbol{r}_j \langle S_i^\eta S_j^\eta(t)\rangle + \cos \boldsymbol{Q}\cdot\boldsymbol{r}_i \cos \boldsymbol{Q}\cdot\boldsymbol{r}_j \langle S_i^\zeta S_j^\zeta(t)\rangle. \tag{7.10.1}$$

For a Bravais lattice within the harmonic approximation, we write the local spin correlation functions in terms of Bose operators using the first system appearing in Eq. (7.9.2)

$$\begin{aligned}\langle S_i^\eta S_j^\eta(t)\rangle &= -\frac{S}{2}\langle a_i a_j(t) - a_i a_j^+(t) - a_i^+ a_j(t) + a_i^+ a_j^+(t)\rangle \\ &= -\frac{S}{2N}\sum_{\boldsymbol{q}} e^{i\boldsymbol{q}\cdot(\boldsymbol{r}_i-\boldsymbol{r}_j)}\langle a_{\boldsymbol{q}} a_{-\boldsymbol{q}}(t) - a_{\boldsymbol{q}} a_{\boldsymbol{q}}^+(t) - a_{\boldsymbol{q}}^+ a_{\boldsymbol{q}}(t) + a_{\boldsymbol{q}}^+ a_{-\boldsymbol{q}}^+(t)\rangle.\end{aligned} \tag{7.10.2}$$

The last line of Eq. (7.10.2) is obtained by the property of the thermal average of the boson operators

$$\langle a_{\boldsymbol{q}} a_{\boldsymbol{q}'}(t)\rangle = \delta_{\boldsymbol{q},-\boldsymbol{q}'}\langle a_{\boldsymbol{q}} a_{-\boldsymbol{q}}(t)\rangle, \quad \langle a_{\boldsymbol{q}}^+ a_{\boldsymbol{q}'}(t)\rangle = \delta_{\boldsymbol{q},\boldsymbol{q}'}\langle a_{\boldsymbol{q}}^+ a_{\boldsymbol{q}}(t)\rangle. \tag{7.10.3}$$

The use of the Bogoliubov transformation (7.2.2) allows us to diagonalize the bilinear Hamiltonian (7.2.1) obtaining the harmonic Hamiltonian (7.2.12) with $A_{\boldsymbol{k}}^{(\mathrm{a})} = 0$. The time evolution of the operators α is then given by Eqs. (3.1.14). From Eq. (7.2.2) and (3.1.14), one obtains

$$\langle a_{\boldsymbol{q}} a_{-\boldsymbol{q}}(t)\rangle = \langle a_{\boldsymbol{q}}^+ a_{-\boldsymbol{q}}^+(t)\rangle = -l_{\boldsymbol{q}}^2 x_{\boldsymbol{q}}[(1+n_{\boldsymbol{q}})e^{i\omega_{\boldsymbol{q}}t} + n_{\boldsymbol{q}} e^{-i\omega_{\boldsymbol{q}}t}], \tag{7.10.4}$$

$$\langle a_{\boldsymbol{q}} a_{\boldsymbol{q}}^+(t)\rangle = l_{\boldsymbol{q}}^2[(1+n_{\boldsymbol{q}})e^{i\omega_{\boldsymbol{q}}t} + x_{\boldsymbol{q}}^2\ n_{\boldsymbol{q}} e^{-i\omega_{\boldsymbol{q}}t}], \tag{7.10.5}$$

$$\langle a_{\boldsymbol{q}}^+ a_{\boldsymbol{q}}(t)\rangle = l_{\boldsymbol{q}}^2[n_{\boldsymbol{q}} e^{-i\omega_{\boldsymbol{q}}t} + x_{\boldsymbol{q}}^2(1+n_{\boldsymbol{q}})e^{i\omega_{\boldsymbol{q}}t}], \tag{7.10.6}$$

where

$$n_{\boldsymbol{q}} = \frac{1}{e^{\beta\hbar\omega_{\boldsymbol{q}}} - 1} \tag{7.10.7}$$

with $\hbar\omega_{\boldsymbol{q}}$ given by Eqs. (7.3.10)–(7.3.12). By the use of Eqs. (7.10.4)–(7.10.6), the correlation function (7.10.2) becomes

$$\langle S_i^\eta S_j^\eta(t)\rangle = \frac{S}{2N}\sum_{\boldsymbol{q}} e^{i\boldsymbol{q}\cdot(\boldsymbol{r}_i-\boldsymbol{r}_j)}\sqrt{\frac{S_{\boldsymbol{q}}}{D_{\boldsymbol{q}}}}[(1+n_{\boldsymbol{q}})e^{i\omega_{\boldsymbol{q}}t} + n_{\boldsymbol{q}} e^{-i\omega_{\boldsymbol{q}}t}], \tag{7.10.8}$$

where $S_{\boldsymbol{q}}$ and $D_{\boldsymbol{q}}$ are given by Eqs. (7.3.11) and (7.3.12), respectively. In a similar way, one obtains

$$\langle S_i^\xi S_j^\xi(t)\rangle = \frac{S}{2N}\sum_{\boldsymbol{q}} e^{i\boldsymbol{q}\cdot(\boldsymbol{r}_i-\boldsymbol{r}_j)}\sqrt{\frac{D_{\boldsymbol{q}}}{S_{\boldsymbol{q}}}}\left[(1+n_{\boldsymbol{q}})e^{iw_{\boldsymbol{q}}t} + n_{\boldsymbol{q}} e^{-iw_{\boldsymbol{q}}t}\right] \tag{7.10.9}$$

$$\langle S_i^\zeta S_j^\zeta(t)\rangle = S^2 - \frac{2S}{N}\sum_{\boldsymbol{q}} l_{\boldsymbol{q}}^2[n_{\boldsymbol{q}} + x_{\boldsymbol{q}}^2(1+n_{\boldsymbol{q}})] \simeq \langle S_i^\zeta\rangle^2. \tag{7.10.10}$$

The last equality of Eq. (7.10.10) is obtained from Eq. (7.3.14). Notice that within the harmonic approximation the correlation $\langle S_i^\zeta S_j^\zeta(t)\rangle$ is time independent. Replacing Eqs. (7.10.8) and (7.10.10) into Eq. (7.10.1), one obtains

$$\begin{aligned}\langle S_i^x S_j^x(t)\rangle &= \sin \boldsymbol{Q}\cdot\boldsymbol{r}_i \sin \boldsymbol{Q}\cdot\boldsymbol{r}_j \frac{S}{2N}\sum_{\boldsymbol{q}} e^{i\boldsymbol{q}\cdot(\boldsymbol{r}_i-\boldsymbol{r}_j)} \\ &\quad\times\sqrt{\frac{S_{\boldsymbol{q}}}{D_{\boldsymbol{q}}}}[(1+n_{\boldsymbol{q}})e^{i\omega_{\boldsymbol{q}}t}+n_{\boldsymbol{q}}e^{-i\omega_{\boldsymbol{q}}t}] \\ &\quad+\cos \boldsymbol{Q}\cdot\boldsymbol{r}_i\ \cos \boldsymbol{Q}\cdot\boldsymbol{r}_j\ \langle S_i^\zeta\rangle^2. \end{aligned} \tag{7.10.11}$$

Similarly, one has

$$\begin{aligned}\langle S_i^y S_j^y(t)\rangle &= \cos \boldsymbol{Q}\cdot\boldsymbol{r}_i\ \cos \boldsymbol{Q}\cdot\boldsymbol{r}_j \frac{S}{2N}\sum_{\boldsymbol{q}} e^{i\boldsymbol{q}\cdot(\boldsymbol{r}_i-\boldsymbol{r}_j)} \\ &\quad\times\sqrt{\frac{S_{\boldsymbol{q}}}{D_{\boldsymbol{q}}}}[(1+n_{\boldsymbol{q}})e^{i\omega_{\boldsymbol{q}}t}+n_{\boldsymbol{q}}e^{-i\omega_{\boldsymbol{q}}t}] \\ &\quad+\sin \boldsymbol{Q}\cdot\boldsymbol{r}_i \sin \boldsymbol{Q}\cdot\boldsymbol{r}_j \langle S_i^\zeta\rangle^2 \end{aligned} \tag{7.10.12}$$

and

$$\langle S_i^z S_j^z(t)\rangle = \frac{S}{2N}\sum_{\boldsymbol{q}} e^{i\boldsymbol{q}\cdot(\boldsymbol{r}_i-\boldsymbol{r}_j)}\sqrt{\frac{D_{\boldsymbol{q}}}{S_{\boldsymbol{q}}}}[(1+n_{\boldsymbol{q}})e^{i\omega_{\boldsymbol{q}}t}+n_{\boldsymbol{q}}e^{-i\omega_{\boldsymbol{q}}t}]. \tag{7.10.13}$$

All other correlation functions do not contribute to the neutron scattering cross-section since the sum over i and j and the exponential factor in Eq. (3.1.2) imply that $S^{\alpha\beta}(\boldsymbol{K},\omega)=0$ for $\alpha\neq\beta$. For $\boldsymbol{Q}\neq 0$ and $\boldsymbol{Q}=\frac{\boldsymbol{G}}{2}$, the only non-zero terms occurring in the structure factor are $S^{xx}(\boldsymbol{K},\omega)=S^{yy}(\boldsymbol{K},\omega)=S_\perp(\vec{\boldsymbol{K}},\omega)$ and $S^{zz}(\boldsymbol{K},\omega)=S_\parallel(\vec{\boldsymbol{K}},\omega)$ where

$$\begin{aligned}S_\perp(\boldsymbol{K},\omega) &= \frac{SN}{8\hbar}\Bigg\{\sqrt{\frac{S_{\boldsymbol{K}-\boldsymbol{Q}}}{D_{\boldsymbol{K}-\boldsymbol{Q}}}}[(1+n_{\boldsymbol{K}-\boldsymbol{Q}})\delta(\omega-\omega_{\boldsymbol{K}-\boldsymbol{Q}})+n_{\boldsymbol{K}-\boldsymbol{Q}}\delta(\omega+\omega_{\boldsymbol{K}-\boldsymbol{Q}})] \\ &\quad+\sqrt{\frac{S_{\boldsymbol{K}+\boldsymbol{Q}}}{D_{\boldsymbol{K}+\boldsymbol{Q}}}}[(1+n_{\boldsymbol{K}+\boldsymbol{Q}})\delta(\omega-\omega_{\boldsymbol{K}-\boldsymbol{Q}})+n_{\boldsymbol{K}+\boldsymbol{Q}}\delta(\omega+\omega_{\boldsymbol{K}+\boldsymbol{Q}})]\Bigg\} \\ &\quad+\frac{(N\langle S_i^\zeta\rangle)^2}{4\hbar}(\delta_{\boldsymbol{K},\boldsymbol{Q}}+\delta_{\boldsymbol{K},-\boldsymbol{Q}})\delta(\omega) \end{aligned} \tag{7.10.14}$$

and

$$S_\parallel(\boldsymbol{K},\omega) = \frac{SN}{2\hbar}\sqrt{\frac{D_{\boldsymbol{K}}}{S_{\boldsymbol{K}}}}[(1+n_{\boldsymbol{K}})\delta(\omega-\omega_{\boldsymbol{K}})+n_{\boldsymbol{K}}\delta(\omega+\omega_{\boldsymbol{K}})]. \tag{7.10.15}$$

The δ-functions with an argument containing the frequency come from the integration over the time present in the structure factor of Eq. (3.1.2). Then the neutron cross-section (3.1.1) becomes

$$\frac{d^2\sigma}{d\Omega dE'} = r_0^2 \frac{k'}{k} \left[\frac{1}{2} g F(\boldsymbol{K})\right]^2 e^{-2W(\boldsymbol{K})} \left[\left(1 + \frac{K_z^2}{K^2}\right) S_\perp(\boldsymbol{K},\omega) + \left(1 - \frac{K_z^2}{K^2}\right) S_\parallel(\boldsymbol{K},\omega)\right], \tag{7.10.16}$$

where $S_\perp(\boldsymbol{K},\omega)$ and $S_\parallel(\boldsymbol{K},\omega)$ are given by Eqs. (7.10.14) and (7.10.15), respectively. Obviously, the term within the square brackets in the neutron cross-section (7.10.16) is invariant if one adds any reciprocal lattice vector $\boldsymbol{G}$ to the scattering wavevector $\boldsymbol{K}$.

The elastic neutron scattering comes from the last term of $S_\perp(\boldsymbol{K},\omega)$ in Eq. (7.10.14). Such a term containing $\delta(\omega)$ is located at $\boldsymbol{K} = \pm\boldsymbol{Q}$ and its intensity is proportional to the square of the order parameter times a geometric factor going from 1 to 2 according to the scattering wavevector $\boldsymbol{K}$ is parallel or perpendicular to the plane in which the spins lie. This contrasts with what happens in collinear systems like ferromagnets or antiferromagnets where the geometric factor vanishes when the scattering wavevector is parallel to the direction of the order parameter. Notice that the location of the elastic peaks gives directly the helix wavevector of the non-collinear phase.

As for the inelastic (one-magnon) neutron scattering cross-section, there are contributions from the creation of a magnon at the expense of the neutron energy corresponding to the terms proportional to $\delta(\omega - \omega_{\boldsymbol{K}})$ and also present at zero temperature, and contributions from the destruction of a magnon which gives its energy to the neutron corresponding to the terms proportional to $\delta(\omega + \omega_{\boldsymbol{K}})$ and present only at non-zero temperature. In any case, for any scattering wavevector $\boldsymbol{K}$, one sees *three* inelastic peaks in correspondence to the frequencies

$$\omega_{\boldsymbol{K}-\boldsymbol{Q}}, \quad \omega_{\boldsymbol{K}+\boldsymbol{Q}}, \quad \omega_{\boldsymbol{K}} \tag{7.10.17}$$

the intensity of which are proportional to

$$\sqrt{\frac{S_{\boldsymbol{K}-\boldsymbol{Q}}}{D_{\boldsymbol{K}-\boldsymbol{Q}}}}, \quad \sqrt{\frac{S_{\boldsymbol{K}+\boldsymbol{Q}}}{D_{\boldsymbol{K}+\boldsymbol{Q}}}}, \quad \sqrt{\frac{D_{\boldsymbol{K}}}{S_{\boldsymbol{K}}}}, \tag{7.10.18}$$

respectively. Notice that from the position of these peaks it is possible to obtain the whole energy spectrum of the spin waves in a non-collinear magnet.

The existence of a DH in the "classical" ground-state energy of the SQ and TR lattices for $j_3 = \frac{1}{2} j_2$, of the HON lattice for $j_3 = 0$, of the FCC lattice for any j' and of the R lattice for $|j'| < 3$, should imply that the isolated elastic peaks become a *ridge* located on the DH line.[70] However, we have seen that the quantum fluctuations destroy the DH line of the "classical" ground state selecting well-defined order wavevectors $\boldsymbol{Q}$ out of the DH manifold (order by quantum disorder). At

the same time, the soft line in the magnon spectrum corresponding to the DH is expected to be replaced by a "rippled soft line", accounting for the contributions to the spectrum from a careful treatment of the terms of the same order in $\frac{1}{S}$ obtained from the normal ordering of the anharmonic terms of the boson Hamiltonian. This challenging calculation is expected to reduce the continuous line of soft modes in the classical spin wave spectrum to a set of discrete soft modes corresponding to the wavevectors $\boldsymbol{k} = \boldsymbol{Q}$ even though the existence of a line of low lying energy excitations may survive. At finite temperature, the modes belonging to the rippled line are thermally populated and a ridge in correspondence of such a line should appear in a quasi-elastic neutron scattering (QENS) experiment.

An analogous scenario was observed[71] in the quasi-2D Heisenberg antiferromagnet K_2NiF_4 ($S = 1$) where the in-plane antiferromagnetic exchange interaction $J_{\rm NN} = -9.68\,{\rm meV}$ is more than 270 times the inter-plane exchange interaction J' and a small uniaxial (Ising) anisotropy $g\mu_B H_A = 0.073\,{\rm meV}$ determines the 2D Ising character of the phase transition at $T_N = 97.2\,{\rm K}$. In this case, the role of the rippled soft line is played by the low energy branch in the spin wave spectrum along the $(0, 0, 1)$ direction that causes the appearance of a ridge in the QENS experiment at temperatures $T = 0.8 - 0.9 T_N$ in addition to the conventional elastic Bragg peaks. The ridge intensity increases as the temperature increases up to T_N. In the paramagnetic phase where the Bragg peaks have been disappeared, the ridge intensity survives up to $2T_N$ even though its intensity decreases with temperature. In K_2NiF_4, the presence of a "Bragg ridge" in addition to "Bragg peaks" is ascribed to the quasi-2D magnetic structure of the system confirmed by the absence of dispersion in the spin wave spectrum along the $(0, 0, 1)$ direction. Indeed, no dispersion of the low lying energy branch at $\hbar\omega(0, 0, k_z) \simeq \sqrt{g\mu_B H_A\ 8|J_{\rm NN}|S} = 2.37\,{\rm meV}$ (at $T = 5\,{\rm K}$) was observed in the INS experiment[71] with an energy resolution of $\sim 0.1\,{\rm meV}$.

The existence of a Bragg ridge profile in the QENS cross-section was observed[72,73] in a polycrystal of solid oxygen in both the monoclinic α ($0 < T < 24\,{\rm K}$) and rhombohedral β ($24 < T < 44\,{\rm K}$) phases. Simultaneous Bragg peaks and ridge-like profile appeared in the QENS cross-section[73] on the α-oxygen with an energy resolution of $\Delta E = 0.06\,{\rm meV}$ while only a similar ridge profile without Bragg peaks was observed in the experiment on the β-oxygen. As for the ordered α-phase, the cross-section profile is ascribed to the low energy magnon branch $10 < \hbar\omega/k_B < 45$ K due to the weak inter-plane exchange interaction[74] in agreement with the K_2NiF_4 scenario. As for the β-phase, one expects the existence of low lying energy branches along both the $(0, 0, 1)$ direction ($0 < \hbar\omega/k_B < 8\,{\rm K}$) and the rippled soft line $\simeq (0, \frac{4\pi}{3a}, k_z)$ ($\hbar\omega/k_B \simeq 0.5\,{\rm K}$) due to the rhombohedral structure of the β-oxygen.[74] Unfortunately, the two contributions cannot be separated owing to the limited energy resolution of the QENS experiment.[73] A support to the simultaneous presence of these two low lying energy branches in the spin wave spectrum is the absence of LRO in the β-phase of the solid oxygen.

A ridge-like structure with Bragg peaks was observed[75] in the rhombohedral $S = \frac{3}{2}$ Heisenberg antiferromagnet $CuCrO_2$ for $T < 25\,\mathrm{K}$. This experiment might be pointed out as a strong evidence for the existence of a quasi-DH in the rhombohedral lattice in addition to a low-lying branch related to the weak inter-plane coupling.